RESPONSE OF RARE EARTH-123 HIGH T_C SUPERCONDUCTORS TO ZINC (II) ION DOPING : POSSIBLE DEPENDENCE ON RARE EARTH ION SIZE

Lt.Jg. NIPAPHAT CHAROENTHAI

A THESIS SUBMITTED IN PARTIAL FULFILMENT

OF THE REQUIREMENTS FOR

THE DEGREE OF MASTER OF SCIENCE (PHYSICAL CHEMISTRY)

FACULTY OF GRADUATE STUDIES

MAHIDOL UNIVERSITY

2000

ISBN 974-664-322-3

Thesis
entitled

RESPONSE OF RARE EARTH-123 HIGH T_C SUPERCONDUCTORS TO ZINC (II) ION DOPING : POSSIBLE DEPENDENCE ON RARE EARTH ION SIZE

Nipaphat Charoenthai
Lt.Jg. Nipaphat Charoenthai
Candidate

Pongtip Winotai
Assoc.Prof. Pongtip Winotai, Ph.D.
Major-advisor

I Ming Tang
Prof. I Ming Tang, Ph.D.
Co-advisor

Sauvarop Limcharoen
Prof. Sauvarop Limcharoen, Dr.rer.nat
Co-advisor

Liangchai Limlomwongse
Prof. Liangchai Limlomwongse,
Ph.D.
Dean
Faculty of Graduate Studies

Sauvarop Limcharoen
Prof. Sauvarop Limcharoen, Dr.rer.nat
Chairman
Master of Science Programme
in Physical Chemistry
Faculty of Science

Thesis
entitled

RESPONSE OF RARE EARTH-123 HIGH T_C SUPERCONDUCTORS TO ZINC (II) ION DOPING : POSSIBLE DEPENDENCE ON RARE EARTH ION SIZE

was submitted to the Faculty of Graduate Studies, Mahidol University
for the degree of Master of Science (Physical Chemistry)
on
May 31, 2000

Nipaphat Charoenthai
.....
Lt.Jg. Nipaphat Charoenthai
Candidate

Pongtip Winotai
.....
Assoc.Prof. Pongtip Winotai, Ph.D.
Chairman

.....
Prof. I Ming Tang, Ph.D.
Member

Srisuda Varamit
.....
Asst. Srisuda Varamit, Ph.D.
Member

Sauvarop Limcharoen
.....
Prof. Sauvarop Limcharoen, Dr.rer.nat
Member

.....
Prof. Liangchai Limlomwongse
Ph.D.
Dean
Faculty of Graduate Studies
Mahidol University

.....
Prof. Amaret Bhumiratana,
Ph.D.
Dean
Faculty of Science
Mahidol University

ACKNOWLEDGEMENTS

I would like to express my sincere gratitude and deep appreciation to my advisors, Assoc. Prof. Dr. Pongtip Winotai and Prof. Dr. I-Ming Tang for their invaluable guidance, advice supervision, encouragement and kindness throughout this research which have enabled me to complete this thesis successfully. I would like to thank Prof. Dr. Sauvarop Limcharoen and Asst. D.r. Srisuda Varamit for their constructive comments and advice about this thesis.

I am also thankful to the Office of Atomic Energy for Peace, for their advice and help with X-ray diffraction . I would like to thank to staff of the Department of Chemistry and Department of Physics, Mahidol University for their co-operation and generous assistance.

I wish to thank the Institute of Science and Technology for Research and Development, Mahidol University, Nakorn Pathom for the financial support in this research. Moreover, my appreciation is also extended to all of my friends and juniors for their moral support and help. Finally, I am deeply grateful to my family for their love, support and encouragement.

Lt.Jg. Nipaphat Charoenthai

4136431 SCPC/M : MAJOR: PHYSICAL CHEMISTRY;
M.Sc.(PHYSICAL CHEMISTRY)
KEY WORDS : HTSC / Orthorhombic distortion / T_c / (d+s) wave theory

Lt.Jg. NIPAPHAT CHAROENTHAI : RESPONSE OF RARE EARTH-123 HIGH T_C SUPERCONDUCTORS TO ZINC(II) ION DOPING : POSSIBLE DEPENDENCE ON RARE EARTH ION SIZE. THESIS ADVISORS: PONGTIP WINOTAI, Ph.D., I MING TANG, Ph.D., SAUVAROP LIMCHAROEN, Dr.rer.nat, 70 p. ISBN 974-664-322-3

The effects of Zn doping in the $REBa_2Cu_{3-x}Zn_xO_{7-y}$ HTSC (RE = Er, Y, Ho, Dy, Gd and Sm) were studied experimentally. X-ray diffraction patterns were taken to determine the effect of Zn doping on the different RE-123 superconductors. Iodometric titration was used to determine the copper valency of all fabricated specimens.

Since one of the aims of the research was to examine the effect of changes in the orthorhombic distortion on the transition temperatures, only specimens having nearly identical copper valency were subjected to detailed measurements. The valencies of specimens studied were in the range between 2.190-2.195. The T_c's were measured and their values were 91.37, 91.82, 92.04, 92.47, 93.10 and 93.26 K respectively.The suppression of T_c's of the different RE-123 due to Zn doping was explained within the framework of a newly developed (d+s)- wave theory for HTSC.

4136431 SCPC/M : สาขาวิชา: เคมีเชิงฟิสิกส์ ; วทม. (เคมีเชิงฟิสิกส์)

เรือโทหญิง นิภาภัทร เจริญไทย:การตอบสนองของสารตัวนำยิ่งยวดอุณหภูมิสูงในระบบแรเอิทร์ท-123 เมื่อแทนที่ด้วยไอออนของสังกะสี: การขึ้นกับขนาดของไอออนของแรเอิทร์ท (RESPONSE OF RARE EARTH –123 HIGH T_C SUPERCONDUCTORS TO ZINC (II) ION DOPING : POSSIBLE DEPENDENCE ON RARE EARTH ION SIZE). คณะกรรมการควบคุมวิทยานิพนธ์: พงศ์ทิพย์ วิโนทัย, Ph.D., อิ มิง ถัง, Ph.D., เสาวรภย์ ลิ้มเจริญ, Dr.rer.nat 70 หน้า. ISBN 974-664-322-3

งานวิจัยนี้เป็นการศึกษาผลของการตอบสนองของสารตัวนำยิ่งยวดอุณหภูมิสูงในระบบแรเอิทร์ท-123(แรเอิทร์ท = เออเบียม อิเทรียม โฮลเมียม ดิสโพรเซียม แกลิโดเนียม และ ซัมมาเรียม) เมื่อแทนที่ด้วยไอออนของสังกะสี โดยการทำ Powder X-ray diffraction ในการตรวจสอบผลการแทนที่ของไอออนของสังกะสีในสารตัวนำยิ่งยวดอุณหภูมิสูงในระบบแรเอิทร์ทต่างๆและใช้วิธี Iodometric titration ในการหาค่าวาเลนซีของทองแดง

จุดประสงค์หนึ่งของการวิจัยคือ การตรวจสอบผลของการเกิด orthorhombic distortion ต่อค่าของ อุณหภูมิวิกฤต (transition temperature) ในสารตัวอย่างที่มีค่าวาเลนซีของทองแดงที่ใกล้เคียงกัน โดยพบว่าค่าวาเลนซีของทองแดงของสารตัวอย่างที่ศึกษามีค่าอยู่ในช่วง 2.190-2.195. ค่าของอุณหภูมิวิกฤตที่วัดได้มีค่าเป็น 91.37, 91.82 ,92.04, 92.47, 93.10 และ 93.26 K ตามลำดับ และพบว่าอัตราการลดลงของอุณหภูมิวิกฤตของระบบแรเอิทร์ท-123 ที่เกิดจากการแทนที่ด้วยไอออนของสังกะสีสามารถอธิบายได้ด้วยทฤษฎี (d+s)-wave.

LIST OF CONTENTS

	Page
ACKNOWLEDGEMENTS	iii
ABSTRACT (English)	iv
ABSTRACT (Thai)	v
LIST OF CONTENTS	vi
LIST OF TABLES	ix
LIST OF FIGURES	x
LIST OF ABBREVIATIONS	xii
CHAPTER I INTRODUCTION	1
1.1 Discovery of Conventional Superconductivity	1
1.1.1 Resistivity	4
1.1.2 Critical Temperature	4
1.1.3 Specific Heat	6
1.2 Theory of Conventional Superconductors	7
1.2.1 Meissner Effect-Diamagnetism	7
1.2.2 Two Fluid Model	8
1.2.3 BCS Theory	9
1.2.4 Anderson Theory	11
1.2.5 Gor'kov Theory	12

LIST OF CONTENTS(Continued)

	Page
1.3 Discovery of High Temperature Superconductors	14
1.3.1 History	14
1.3.2 Properties	16
1.3.3 Properties which Contradict Conventional Theory	17
CHAPTER II REVIEW AND AIM TO STUDY	18
2.1 Characteristics and Structure of 123-Compounds	18
2.2 Review of Experimental Results of 123-Compounds	22
2.2.1 Hole Concentration Dependence	22
2.2.2 Rare Earth Substitution	23
2.2.3 Transition Metal Substitution	24
2.3 Aim to Study	26
2.4 Method of Research	27
CHAPTER III EXPERIMENTAL METHODS	28
3.1 Instrumentation	28
3.2 Chemicals	29
3.3 Calculation the Stoichiometric Amount of Chemical Compound	29
3.4 Preparation of Ceramic Samples	30
3.5 Sintering Process	31

LIST OF CONTENTS(Continued)

	Page
3.6 Characterization	34
3.6.1 Powder X-ray Diffraction	34
3.6.2 Iodometric Titration	35
3.6.3 Four-Probe Method	36
3.7 Flow Diagram of Experimental Procedures	39
CHAPTER IV RESULTS	40
4.1 Copper Valency	40
4.2 Results From Powder X-Ray Diffraction	44
4.3 Critical Temperature	47
CHAPTER V DISCUSSION AND CONCLUSION	51
REFERENCE	55
APPENDIX A	59
APPENDIX B	63
BIOGRAPHY	70

LIST OF TABLES

Table	Page
1.1 The transition temperature T_c and critical magnetic field for superconducting elements	2
1.2 Year of discovery and critical temperature T_c of some superconductors	15
4.1 Lattice parameters, orthorhombic distortion (D), copper valency and T_c of $ErBa_2Cu_{3-x}Zn_xO_{7-y}$	41
4.2 Lattice parameters, orthorhombic distortion (D), copper valency and T_c of $YBa_2Cu_{3-x}Zn_xO_{7-y}$	41
4.3 Lattice parameters, orthorhombic distortion (D), copper valency and T_c of $HoBa_2Cu_{3-x}Zn_xO_{7-y}$	42
4.4 Lattice parameters, orthorhombic distortion (D), copper valency and T_c of $DyBa_2Cu_{3-x}Zn_xO_{7-y}$	42
4.5 Lattice parameters, orthorhombic distortion (D), copper valency and T_c of $GdBa_2Cu_{3-x}Zn_xO_{7-y}$	43
4.6 Lattice parameters, orthorhombic distortion (D), copper valency and T_c of $SmBa_2Cu_{3-x}Zn_xO_{7-y}$	43

LIST OF FIGURES

Figure	Page
1.1 Resistance in Ohms of a specimen of mercury versus absolute temperature	2
1.2 Experimental threshold curves of the critical field $H_c(T)$ versus temperature for several superconductors	4
1.3 Meissner effect in a superconducting phase cooled in a constant applied magnetic field	7
1.4 Magnetization versus applied magnetic field for a bulk superconductor (a) Type I superconductor (b) Type II superconductor	8
1.5 The evolution of critical temperatures since the discovery of superconductivity	15
2.1 Schematic diagrams of (a) $YBa_2Cu_3O_6$ and (b) $YBa_2Cu_3O_7$	18
2.2 Schematic structure of $YBa_2Cu_3O_{7-y}$	19
2.3 Variation of the critical temperatures upon doping in $YBa_2Cu_3O_{7-y}$	21
2.4 Schematic phase diagram of a cuprate superconductor	21
2.5 A model unit of layered $YBa_2Cu_3O_{7-y}$	22
3.1 Typical program showing heating steps for calcination	32
3.2 Typical program showing heating steps for sintering	32
3.3 The compactor unit for pressed pellet	33
3.4 Connection of sample and probe	37

LIST OF FIGURES (Continued)

Figure	Page
4.1 Variation of copper valency with mole fraction of Zn	40
4.2 X-ray diffraction pattern of $GdBa_2Cu_{3-x}Zn_xO_{7-y}$	45
4.3 Variation of orthorhombic distortion with ionic radiusn of rare earth in $REBa_2Cu_{3-x}Zn_xO_{7-y}$ (RE = Er, Y, Ho, Dy, Gd and Sm)	46
4.4 Temperature dependence of the resistivity of $ErBa_2Cu_{3-x}Zn_xO_{7-y}$	47
4.5 Depression T_c of $ErBa_2Cu_{3-x}Zn_xO_{7-y}$ with mole fraction of Zn	48
4.6 Depression T_c of $YBa_2Cu_{3-x}Zn_xO_{7-y}$ with mole fraction of Zn	48
4.7 Depression T_c of $HoBa_2Cu_{3-x}Zn_xO_{7-y}$ with mole fraction of Zn	49
4.8 Depression T_c of $DyBa_2Cu_{3-x}Zn_xO_{7-y}$ with mole fraction of Zn	49
4.9 Depression T_c of $GdBa_2Cu_{3-x}Zn_xO_{7-y}$ with mole fraction of Zn	50
4.10 Depression T_c of $SmBa_2Cu_{3-x}Zn_xO_{7-y}$ with mole fraction of Zn	50
A.1 Diagram for (a) diagonal propagator (b) off- diagonal propagator	62
A.2 Diagram for non-spin flip scattering (a) diagonal (b) off- diagonal	63
A.3 Diagram for spin flip scattering (a) diagonal (b) off- diagonal	64

LIST OF ABBREVIATIONS

R, ρ	Resistivity
T_c	Critical or transition temperature
T	Temperature
H_c	Critical magnetic field
B	Applied magnetic field
k_B	Boltzman Constant
HTSC	High temperature Superconductor
LSCO	$La_{2-x}Sr_xC_uO_4$
YBCO	$YBa_2Cu_3O_{7-y}$
BCS	Bardeen-Cooper-Schrieffer
G.F.	Green function
OP	Order parameter
TM	Transition metal
RE	Rare earth element
RE-123	$REBa_2Cu_3O_{7-y}$
XRD	Powder X-ray diffraction
LSF	Local spin fluctuation
2D	Two dimensions
emf	Electromotive force
D	Orthorhombic distortion

CHAPTER I

INTRODUCTION

1.1 Discovery of Conventional Superconductors

In 1908, Heike Kammerlingh Onnes liquified helium He^4 by repeatly throttling gaseous helium. Having liquid helium, Onnes began to do various experiments in 1911. He discovered that the resistivity of mercury suddenly drops to zero whenever the sample was cooled to below 4.2 K, the boiling point of liquid helium. This phenomenon was called superconductivity. The temperature T_c at which resistivity dropped almost to zero was taken to be the temperature at which the transition from the normal conducting phase into a new conducting phase in which R = 0.The new phase was labelled the superconducting phase [1]. In the years following it was discovered that many other metallic elements also exhibited superconductivity at very low temperature.(Table 1.1) [2]. In 1913 the element lead was found to be superconducting at 7.2 K, while in 1930 the highest critical temperature of all pure metal was discovered in Nb, T_c = 9.2 K. Higher transition temperature occurred in the alloys such as Nb_3Sn, T_c = 18.05 K.

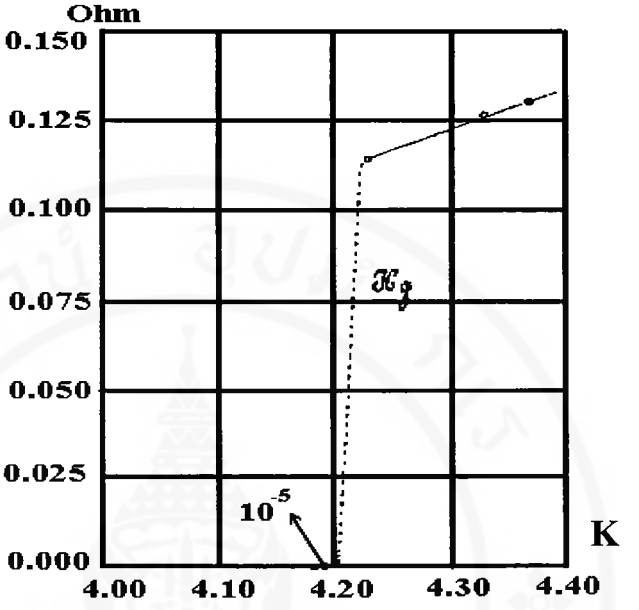

Figure 1.1 Resistance in Ohms of a specimen of mercury versus absolute temperature.

Table 1.1 The transition temperature T_c and critical magnetic field for superconducting elements

Elements	Transition temperature (K)	Critical magnetic field (10^{-4} Tesla)
Ti	0.390	100
Al	1.140	105
Zn	0.875	53
Ga	1.091	51
Nb	9.500	1980
Pb	7.193	803

1.1.1 Resistivity

The resistivity of a superconductor to direct current is zero as far as it can be measured. Zero resistivity is observed in a superconductor at all temperatures below the critical temperature, T_c (see in Figure 1.1). However, if we passs a current higher than the critical current density J_c, superconductivity will disappear. Above room temperature, the resistivity of most metals is approximately a linear function of temperature. In general, the resistivity of any substance is expected to go as [3]

$$\rho = \rho_0\left(1 + \alpha T + \beta T^2 + ... + \gamma T^n + ...\right) \qquad (1.1)$$

where each temperature dependence is a reflection of a scattering mechanism. Real metal contains some imperflections and so one observes some finite resistivity at low temperatures. This resistivity, extrapolated to T = 0, is called the residual resistivity, ρ_0. As we increase the temperature, the electrons also gets scattered by thermals of the lattice (called phonon) so the resistivity rises with temperature. This contribution is called phonon resistivity $\rho_p(T)$. Therefore the temperature dependence of resistivity described as

$$\rho(T) = \rho_0 + \rho_P(T) \qquad (1.2)$$

1.1.2 Critical magnetic field

In addition to zero resistivity, the superconductors exhibit another property. A sufficiently strong magnetic field can destroy the superconducting phase. The value of magnetic field at which superconductivity is destroyed is called the critical magnetic field H_c. This field H_c is a function of temperature. Close to critical temperature T_c, only a small field is needed to destroy superconductivity [3]. The temperature dependence closed to T_c is

$$H_c(T) = H_c(0)\left[1-\left(\frac{T}{T_c}\right)^2\right] = 1.73H_c(0)\left[1-\left(\frac{T}{T_c}\right)\right] \quad (1.3)$$

where $H_c(0)$ is the extraporated critical field at T = 0 K

The variation of the critical field with temperature for several superconducting element is shown in Figure 1.2 [1]. A specimen is superconducting below the curve and normal above the curve. For pure metal superconductors like Sn, Pb, In, Al, etc., $H_c(0)$ is of order a few hundred Guass. In alloy superconductors like Nb_3Sn, superconductivity may persist in regions even in fields of about 10^5 Gauss.

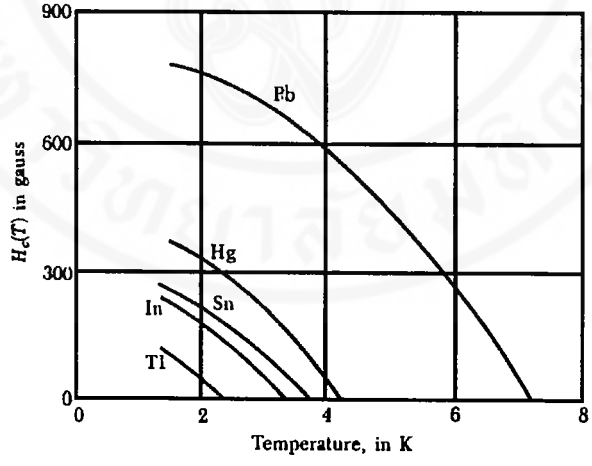

Figure 1.2 Experimental threshold curves of the critical field $H_c(T)$ versus temperature for several superconductors.

1.1.3 Specific heat

One of the most extensively studied properties of superconductors is the specific heat. The specific heat of a superconductor consists, like that of a normal metal of two contributions [3]

$$C = C_{latt} + C_{el} \tag{1.4}$$

where C_{latt} is lattice specific heats and must be the same in both the superconducting and normal states and where C_{el} is electronic specific heat and is different in the superconducting and normal states, i.e.

$$C_s - C_n = \left(C_{el}\right)_s + \left(C_{el}\right)_n \tag{1.5}$$

The specific heat of a normal state at low temperature has the form

$$C_n = \gamma T + AT\left(\frac{T}{\Theta}\right)^3 \tag{1.6}$$

where γ is the Sommerfeld constant , which is proportional to the density of electric states at the Fermi surface, Θ is the Debye temperature, and A is a numerical constant for all metals. From the above equation the linear term is the electronic contribution to the specific heat and the cubic term is the contribution from the lattice vibration. In general, $\gamma >> (A / \Theta^3)$ and so the cubic dependence is seen at high temperature while the linear dependence is seen at low temperature. When plotting C/T versus T^2 should give a straight line whose slope is A / Θ^3 and intercept is γ. Hence, from measurements on the superconductor in the normal state, i.e. by applying a magnetic field greater than H_c, we can determine the lattice specific heat, $C_{latt} = A(T/\Theta)^3$. The specific heat of the lattice is the same in both the superconducting and mormal states, so, by subtracting the value of C_{latt} from the total specific heat of the superconducting state,

we can obtain the electronic contribution $(C_{el})_s$. This points to the superconducting state involving some quite drastic change in the behavior of the conduction electrons. $C_{(el)s}$ can be represented by the equation

$$\frac{C_{(el)s}}{\gamma T_c} = ae^{(-b/T)} \tag{1.7}$$

where a and b are numerical constant for each metals [3].

1.2 Theory of Conventional Superconductors

1.2.1 Meissner effect – diamagnetism

Up to 1933, the phenomenon seen by Onnes was believed to be a manifestation of perfect conductivity. However, the experiment performed by Meissner and Ocshenfeld carried out for perfect conductivity showed that the phenomenon was connected to perfect diamagnetism and not to perfect conductivity. It is an experimental fact that a bulk superconductor in a weak magnetic field will act as a perfect diamagnet, with zero magnetic induction in the interior. When a specimen is placed in a magnetic field and is then cooled through the transition temperature to superconductivity, the magnetic flux originally present is ejected from the specimen. The effect B = 0 in superconductor is called the Meissner effect, as was already illustrated in Figure1.3[1].

The Meissner–Ochsenfeld effect cannot be deduced from the infinite conductivity of superconductor. The exclusion of the magnetic field from the interior of a superconducting specimen is direct evidence that the superconducting state is not simply one of zero resistance [2]. The magnetization curve expected for a

superconductor under the condition of the Meissner-Ochsenfeld experiment is sketched in Figure 1.4 [1].

Pure specimen of materials such as Sn, Pb exhibits a complete Meissner effect in Figure 1.4 (a), they are called type I (soft) superconductor. Other materials exhibit a magnetization curve of the form of Figure 1.4(b) and are known as type II (hard) superconductor. They tend to be alloy or transition metal. Between the lower critical field H_{c1} and the upper field H_{c2} the flux density $B \neq 0$ and the Meissner effect is said to be incomplete and this region is called the vortex state [1].

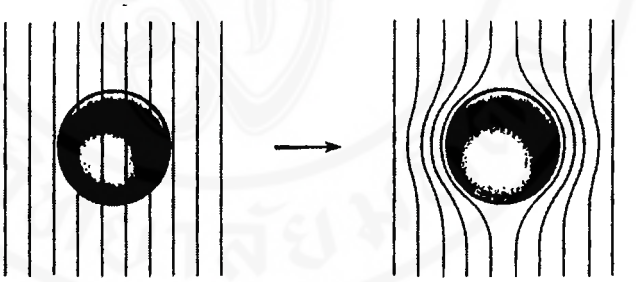

Figure 1.3 Meissner effect in a superconducting phase cooled in a constant applied magnetic field

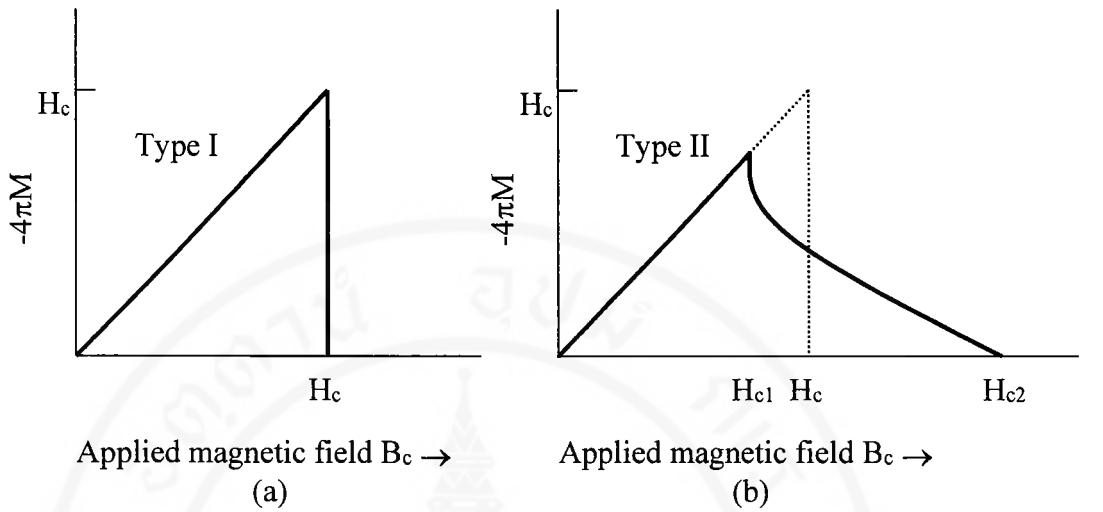

Figure 1.4 Magnetization versus applied magnetic field for a bulk superconductor

(a) Type I superconductor (b) Type II superconductor

1.2.2 Two fluids theory

One of the simplest ideas which was put forward in 1934 for describing superconductivity was the "two fluids" model of Gorter and Casimir. This model has two general assumptions [3]

1. The system exhibiting superconductivity posses as an order or condensed state, the ordering being described by an order parameter. This parameter is taken to vary from zero at $T = T_c$ to unity at $T = 0$ K.

2. The entire entropy of the system is due to the disorder of non-condensed individual excited particles, the behavior is taken to be similar to the equivalent particles in the normal state.

Gorter and Casimir assumed that a superconductor below its transition temperature appears as two types electron fluids, one of super electrons with a fraction

x and one of normal electrons with the fraction (1-x). Since the superconducting transition is a transition of second order, the total Helmholtz energy of superconductor would be given by [4]

$$F(T) = xF_s + (1-x)^r F_n T \qquad (1.8)$$

where $F_s = -H_0^2 / 8\pi$, $F_n = -(1/2)\gamma T^2$ where γ is the usual coefficient defining the electronic specific heat , r = some adjustable parameter chosen to be 1/2. In that case, minimization of the free energy from above equation with respect to x leads to

$$x(T) = 1 - t^4 \quad ; \quad t = \frac{T}{T_c} \qquad (1.9)$$

That is the number of normal electrons falls very rapidly below T_c, with a corresponding rapid rise in the number of condensed electrons. This model predicts the specific heat that

$$C_{(el)s} = 3\gamma T_c t^3 \qquad (1.10)$$

and corresponding the critical field curve is

$$H_c = H_c(0)\,[1-t^2] \qquad (1.11)$$

1.2.3 Bardeen, Cooper, Schrieffer (BCS) theory

Each electron has an energy ε and momentum p. The wave function for an electron shall satisfy certain boundary conditions, there is a finite number of eigenstates in a given energy range, each eigenstate having an energy ε and momentum p as well defined as the uncertainty principle permits. The probability that the given eigenstate is occupied by an electron is given by the Fermi-Dirac distribution [3]

$$f(\varepsilon) = \frac{1}{e^{(\varepsilon-\varepsilon_F)/kT} + 1} \qquad (1.12)$$

where ε_F is the Fermi energy. At absolute zero, the Fermi-Dirac function takes the form of a step-function. A microscopic theory of superconductivity was developed by Cooper [5]. Cooper showed that the effective attraction between electrons near the Fermi surface due to the electron-phonon interaction, must lead to bound pairs of electrons, regardless of how weak the attraction may be. The Cooper pair is composed of a spin up and spin down electron.

In 1957 Bardeen, Cooper, and Schrieffer (BCS) [6] were able to apply this to a system of many interacting electrons. The fundamental assumption of the BCS theory is that the attractive interaction was due the electron-phonon pairing interaction. The BCS theory has been found to described all superconductive phenomena in weakly coupled superconductors, which have $2\Delta << \varepsilon_F$. In weak-coupling the energy gap is related to the transition temperature by [7]

$$\Delta(0) = 1.764 k_B T_c = 2\hbar\omega_D e^{\left[\frac{-1}{N(\varepsilon_F)V}\right]} \qquad (1.13)$$

where ω_D is the lattice Debye frequency. Near T_c the half-gap is expected to decrease as

$$\Delta(T) \approx 1.74\Delta(0)(1-t)^{1/2} \quad ; \quad t = \frac{T}{T_c} \qquad (1.14)$$

In ground state, all electrons are paired. By breaking the pair one introduces excitations. Excitations are introduced by taking an electron from below the Fermi surface to fill a state above it. If electron energy is close to the Fermi surface, energy difference can be very small. There is a minimum change to energy 2Δ required to break up a pair [2].

1.2.4 Anderson theory

In 1959 P.W.Anderson [8] established a theorem that addition of nonmagnetic impurities (e.g.Zn($3d^{10}$)) to conventional superconductors does not changes any of it superconducting transition. His work was based on a Green's function approach to BCS theory in which exist both a normal and anomalous Green's function.

In the presence of any perturbation, the Green's function will have a similar form to that of the unperturbed stated except that ω and Δ will be replaced by an renormalized frequency and an unrenormalized energy gap [not order parameter] determined by Dyson's equation. In the normal superconductors, ones find that nonmagnetic impurities give the same corrections to the diagonal part and off-diagonal part because there is non-spin flip scattering. Then analytic expression diagonal term is

$$\tilde{\omega} = \omega + N(0)|U_N|^2 \frac{\tilde{\omega}}{\sqrt{\tilde{\omega}^2 + |\Omega|^2}} \tag{1.15}$$

$$\tilde{\omega} = \omega + \frac{1}{2\tau_N} \frac{\tilde{\omega}}{\sqrt{\tilde{\omega}^2 + |\Omega|^2}} \tag{1.16}$$

and off-diagonal term is

$$\Omega = \Delta_{op} + \frac{1}{2\tau_N} \frac{\Omega}{\sqrt{\tilde{\omega}^2 + |\Omega|^2}} \tag{1.17}$$

where N(0) is the density of states of one spin in the normal metal at the Fermi surface, U_N is the normal scattering potential and τ_N is the normal scattering life times. From a concept borrowed from high-energy physics and statistical mechanics we have

$$\tilde{\omega} = Z\omega \quad \text{and} \quad \Omega = Z\Phi$$

where Z is an renormalization constant and Φ is an renormalized energy gap.

The renormalized constant Z of diagonal and off diagonal corrections is given by equation (1.18) and (1.19)

$$Z\omega = \omega + \frac{1}{2\tau_N}\frac{\omega}{\sqrt{\omega^2 + |\Phi|^2}} \tag{1.18}$$

$$Z\Phi = \Delta_{op} + \frac{1}{2\tau_N}\frac{\omega}{\sqrt{\omega^2 + |\Phi|^2}} \tag{1.19}$$

Dividing equation (1.18) by ω and multiply by Φ we get

$$Z\Phi = \Phi + \frac{1}{2\tau_N}\frac{1}{\sqrt{\tilde{\omega}^2 + |\Omega|^2}} \tag{1.20}$$

Substracting equation (1.19) and (1.20) by two side and divided by frequency $1/\omega$ we get

$$\frac{\Phi}{|\omega|} = \frac{\Delta_{op}}{|\omega|} \tag{1.21}$$

If the energy gap goes to zero, the order parameter goes to zero. Then normal scattering by impurity does not change superconductivity.

1.2.5 Gor'kov theory

L.P. Gor'kov and A.A. Abrikosov [9] gave a very successful theory of the effect of magnetic impurities on superconductivity. They prove that magnetic impurities (through spin flip scattering) will destroy superconductivity. The magnetic moments on these impurities flip one of the spins in the Cooper pair. Again their work was based on BCS theory and also used Green's function the same as Anderson theory. But in magnetic impurities, the correction to the off-diagonal part as a minus sign and

is different from the correction to the diagonal part because there is spin flip scattering. Then we get analytic expression diagonal term is

$$\tilde{\omega} = \omega + \frac{1}{2\tau_S} \frac{\tilde{\omega}}{\sqrt{\tilde{\omega}^2 + |\Omega|^2}} \tag{1.22}$$

And the off-diagonal term is

$$\Omega = \Delta_{op} - \frac{1}{2\tau_S} \frac{\Omega}{\sqrt{\tilde{\omega}^2 + |\Omega|^2}} \tag{1.23}$$

where τ_S is the spin flip scattering life times. The renormalized constant Z of diagonal and off-diagonal correction is given by equation (1.24) and (1.25)

$$Z\omega = \omega + \frac{1}{2\tau_S} \frac{\omega}{\sqrt{\omega^2 + |\Omega|^2}} \tag{1.24}$$

$$Z\Phi = \Delta_{op} - \frac{1}{2\tau_S} \frac{\Phi}{\sqrt{\omega^2 + |\Omega|^2}} \tag{1.25}$$

Dividing equation (1.24) by ω and multiplying by Φ both sides we get

$$Z\Phi = \Delta_{op} - \frac{1}{2\tau_S} \frac{\Phi}{\sqrt{\omega^2 + |\Omega|^2}} \tag{1.26}$$

Substracting equation (1.25) and (1.26) then we get

$$\Phi = \frac{\Delta_{op}}{1 + \frac{1}{\tau_S} \frac{1}{\sqrt{\omega^2 + |\Phi|^2}}} \tag{1.27}$$

Dividing equation (1.27) by frequency $1/\omega$ we get

$$\frac{\Phi}{|\omega|} = \frac{\Delta_{op}}{\omega + \frac{1}{\tau_S} \frac{\omega}{|\omega|}} = \frac{\Delta_{op}}{\omega + \frac{1}{\tau_S} \operatorname{sgn} \omega} = \frac{\Delta_{op}}{\omega + n_i \alpha} \tag{1.28}$$

where n_i is the impurities concentration.

1.3 Discovery of High Temperature Superconductors

1.3.1 History

The field of high temperature superconductivity (HTSC) is a relatively new one, only thirteen years old. It began with the discovery of superconductivity in $La_{2-x}Ba_xCuO_{4-\delta}$ at 35 K by K.A.Muller and J.G.Bednorz in 1986. First paper [10] entitled, " Possible High T_c Superconductivity in the Ba-La-Cu-O System". This discovery did not generate much excitement since a T_c of 35 K still requires the use of liquid helium. Thereafter Chu et al.[11], Hikami et al.[12] and Zhao et al.[13] discovered of 90 K superconductivity in the Y-Ba-Cu-O ceramic compounds in 1987. This created the enormous excitement since at 90 K, liquid nitrogen which is cheap and plentiful could be used to achieve the requierd temperatures needed. Researchers were started to find that replacing La by the smaller Y raises the onset temperature above the temperature of liquid N_2 to 92 K [14,15]. Superconductivity above 100 K was obtained in the Bi-Sr-Ca-Cu-O system [16]. More recently, Sheng and Herman [17,18] discovered superconductivity near 120 K in the Tl-Ba-Ca-Cu-O system. In a closely related system have obtained a transition to superconductivity at the current record temperature of 125 K [19]. Several researchers have reported T_c above 130 K for the Hg series of compound $HgBa_2Ca_nCu_{n+1}O_{2n+4}$ with n = 1,2 [20,21].

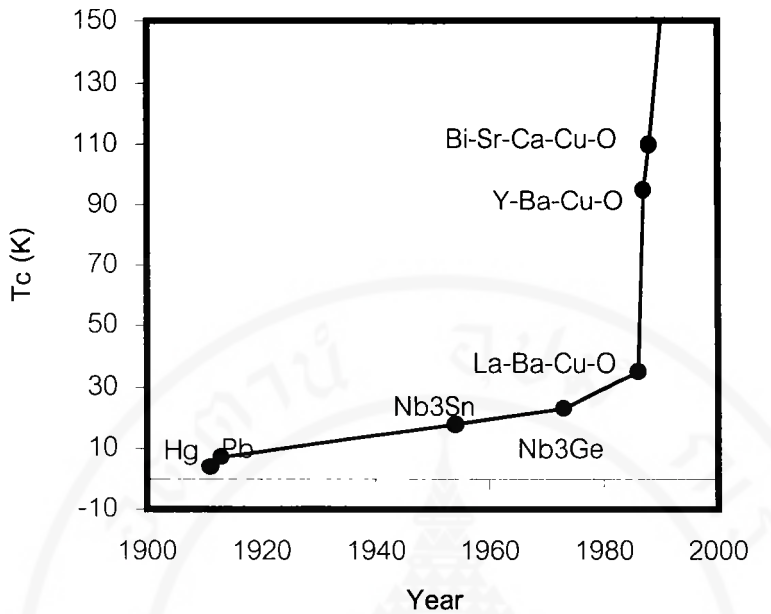

Figure 1.5 The evolution of critical temperatures since the discovery of superconductivity.

Table 1.2 Year of discovery and critical temperature T_c of some superconductors

Material	T_c (K)	Year
Hg	4.1	1911
Pb	7.2	1913
Nb	9.2	1930
Nb_3Sn	18.1	1954
Nb_3Ga	20.3	1971
Nb_3Ge	23.2	1973
$Ba_xLa_{5-x}Cu_5O_y$	30-35	1986
$YBa_2Cu_3O_{7-y}$	95	1987
$Bi_2Sr_2Ca_2Cu_3O_{10}$	110	1988
$Tl_2Ba_2Ca_2Cu_3O_{10}$	125	1988
$Hg_{0.8}Pb_{0.2}Ba_2Ca_2Cu_3O_x$	133	1993

1.3.2 Properties

Except for some materials (like $Ba_{1-x}K_xBiO_3$), most high T_c superconducting oxides are cuprate compounds. One of their characteristics is the presence of CuO_2 layers which dominate most properties. The original materials, $La_{2-x}Sr_xCuO_4$ (LSCO) and $YBa_2Cu_3O_7$ (YBCO) consist of layered cuprate structure. High T_c superconducting oxides also contains grains, grain boundaries, twins, voids and other imperfections. It may well turn out that various imperflections found in HTSC crystals are intrinsic to these materials. Their critical temperature are about 100 K and need very high magnetic fields to completely destroy superconductivity (~100 Tesla at 4.2 K) [2]. Oxygen stoichiometry significantly affects the properties of the high temperature superconductors. Cava found that in the Y-Ba-Cu-o system [22] a plateau in T_c and a minimum in the room temperature resistivity as a function of oxygen concentration. HTSC has very short coherence length: $\xi \sim 10$ Å, which is comparable to the size of the unit cell, and it has profound consequences for the physics of HTSC oxides. Short coherence length also implies that HTSC oxides are type-II superconductors with very high upper critical fields B_{c2}. One of the unusual features of HTSC compounds is the fact that they are very close to an insulating phase. The insulator is slightly doped in order to obtain the superconducting state. If the doping is increased, superconductivity disappears [2].

1.3.3 Properties which contradict conventional theory

The cuprate oxide high temperature superconductors (HTSC) are considered to be unconventional superconductors. The replacement of the Cu ions in HTSC's by other transition metal ions, both magnetic (Ni^{2+}, Fe^{3+} and Co^{3+}) and non magnetic (Zn^{2+} and Al^{3+}) ions, found that both the magnetic and non magnetic transition metal ions substitutions suppress the superconductivity. Even more surprising was the fact that the suppression of T_c by Zn^{2+} ion substitution is greater than that due to Ni^{2+} ion substitution. The observed response to the two types of impurities, magnetic Ni^{2+} and non magnetic Zn^{2+} ions, is the exact opposite of what is predicted by the conventional theory of superconductivity. One of the first theories established by P.W.Anderson [8] is the theory which states that the doping of non magnetic zinc in a superconductor host leads to negligible changes. Another theory, the Abrikosov-Gor'kov theory [9], states that paramagnetic impurities suppresses superconductivity though their breaking of the Cooper pair and that this leads to a rapid (total) suppression of superconductivity. To explain the observed responses, a new mechanism for pair condensation in the HTSC's is required. An indication of their unconventionality is the symmetry of their order parameter (OP). Another indication of the unconventionality is the response of the HTSC to magnetic and non magnetic transition metal (TM) doping, i.e., they are opposite of the responses of conventional superconductors to the same TM doping [23,24].

CHAPTER II

REVIEW AND AIM TO STUDY

2.1 Characteristics and Structure of 123-Compounds

$YBa_2Cu_3O_7$ is usually referred to as YBCO or as 123. It has entered into history as the first material with critical temperature above the boiling point of liquid nitrogen (77 K). However, its correct formula reads $YBa_2Cu_3O_{7-y}$ and its structure and properties depend on the oxygen concentration. The structure of $YBa_2Cu_3O_{7-y}$ is based on a tetragonal perovskite tripled along the c-axis. If we observe the structure in Figure 2.1 we notice that the structure consists of a sequence of oxide layer perpendicular to the c-axis.

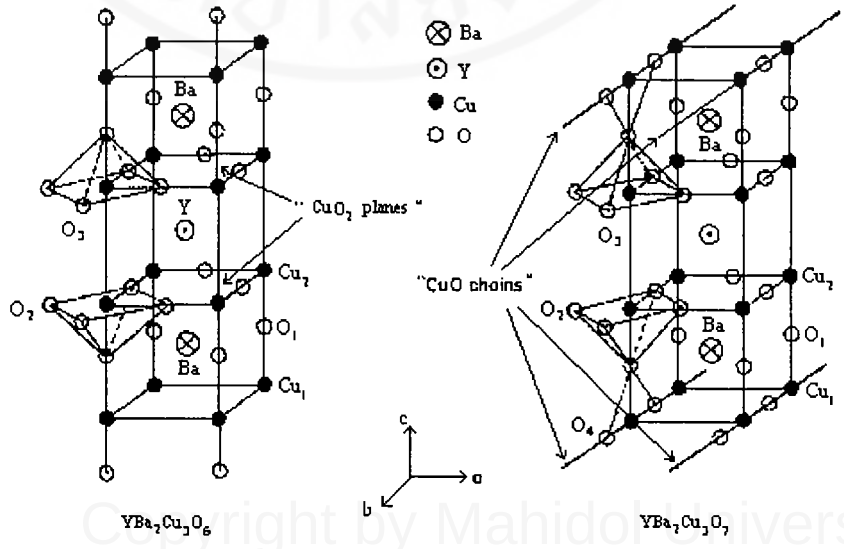

Figure 2.1 Schematic diagrams of (a) $YBa_2Cu_3O_6$ and (b) $YBa_2Cu_3O_7$

As shown in Figure 2.2, the structure of YBCO can be represented as a layered structure that consists of two CuO_2 planes seperated by Y site.

----------Cu-O chain or Cu(1) site----------

BaO

---------CuO_2 plane or Cu(2) site----------

Y

---------CuO_2 plane or Cu(2) site----------

BaO

----------Cu-O chain or Cu(1) site----------

Figure 2.2 Schematic structure of $YBa_2Cu_3O_{7-y}$

From Figure 2.1 and 2.2, copper can be found in two different sites: Cu(1) within square,CuO_4 and Cu(2) within a square-based pyramid, CuO_5. The separation of yttrium ions gives the structure a two-dimensional character [2]. Combined thermogravimetric and X-ray studies [25] show that the oxygen ions on the a-axis between the Cu ions in the middle copper layer are the first to leave as the ceramic is being heated. The absence of these O ions causes the distortion [26] which leads to the orthorhombic structure occurring in these ceramics. Since each of these oxygen ions are shared by two unit cells, their absence leads to the chemical composition $YBa_2Cu_3O_7$. In these composition , one has a layer containing linear chains of Cu-O occurring along the b-axis sandwiched between two 2-dimensional Cu-O layers. Removal of additional oxygen ions from the b-axis linking the Cu ions on the middle

copper layer results in the composition $YBa_2Cu_3O_{7-y}$. The oxygen content per cell can be changed reversibly from 7.0 to 6.0 atoms, simply by pumping oxygen in and out of the parallel chains of CuO that run along the b-axis of the Figure 2.1. At the composition $YBa_2Cu_3O_6$ the crystal in an insulator (tetragonal phase), which is antiferromagnetic. An increase in oxygen above $O_{6.5}$ makes the crystal metallic and non-magnetic; the crystal then enters into the superconducting phase as more oxygen is added. The charge-neutral formula for $YBa_2Cu_3O_7$ can be written as $YBa_2 (Cu^{2+})_2 (Cu^{3+})(O^{2-})_7$ or as $YBa_2(Cu^{2+})_3(O^{2-})_6(O^-)$. The exact orthorhombic (quasi-tetragonal) cell dimensions of $YBa_2Cu_3O_7$ are a = 3.88 $\mathring{A}$, b = 3.84 $\mathring{A}$, c = 11.63 $\mathring{A}$, with a cell volume ~ 173 $\mathring{A}^3$ [1].

In the undoped compound, the Cu ions (2+) in this plane are in a d^9 electronic configuration and are antiferromagnetically coupled to other neighboring copper ions, and the plane is insulating. The Cu-O chains can be considered as a charge-reservoir which transfers the charge into CuO_2 planes. Charge carriers can also be added by doping : basically by substituting divalent atoms for trivalent ones (like Sr^{2+} for La^{3+} in $La_{2-x}Sr_xCuO_4$) or by adding oxygen to $YBa_2Cu_3O_6$, which enters the compound as O^{2-} and form Cu-O chains. To maintain the charge balance, electrons are removed from the copper oxide planes and the remaining holes (missing electrons) are mobile (conduction) and they form Cooper pairs below T_c (superconductivity). So we can understand that adding charge carriers from the reservoir into the CuO_2 planes gradually increases the conductivity within the ab-plane. While the conductivity seems to increase first, reach in maximum for some optimal doping, then decrease and finally vanish for about 0.3 holes per Cu (see Figure 2.4) [2].

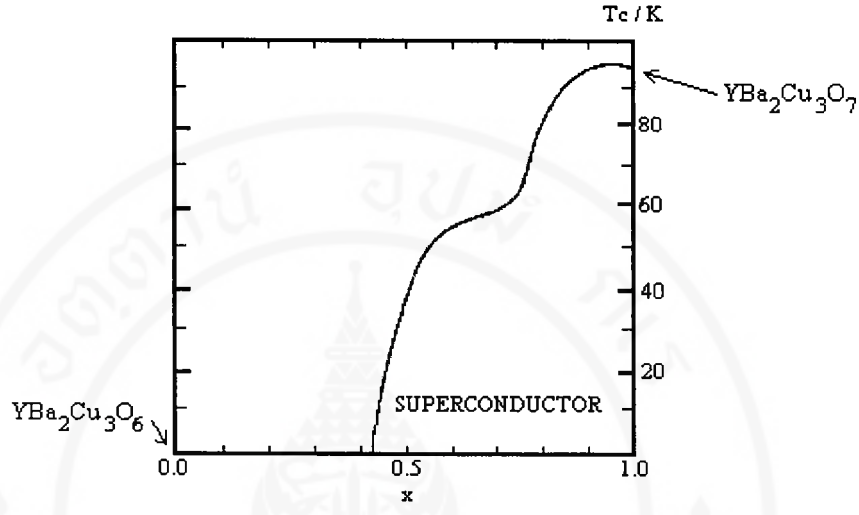

Figure 2.3 Variation of the critical temperature upon doping in $YBa_2Cu_3O_{7-y}$

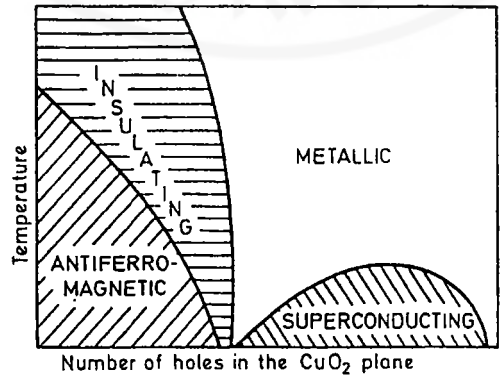

Figure 2.4 Schematic phase diagram of a cuprate superconductor

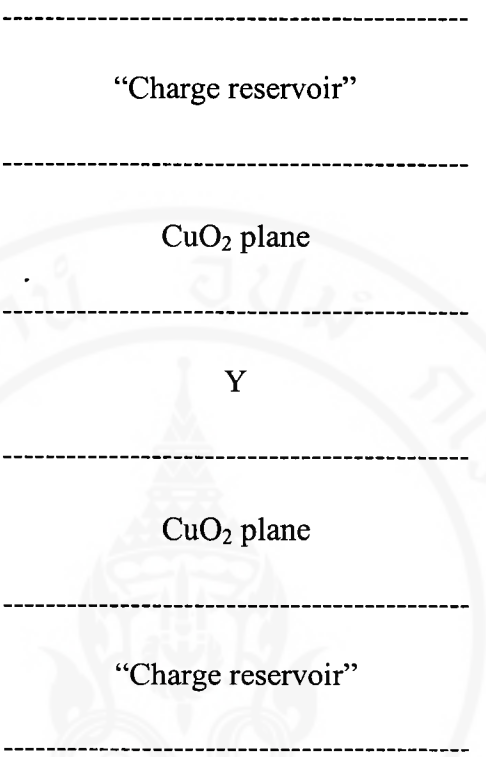

Figure 2.5 A model unit of layered $YBa_2Cu_3O_{7-y}$

2.2 Review of Experimental Results of 123-Compounds

2.2.1 Hole concentration dependence

It is now accepted that the single most important factor needed for achieving higher T_c's in the copper oxide perovskite structure superconductors is the optimization of the hole concentration(copper valency) in the two-dimensional CuO_2 plane of the ceramics. The holes can be created when excess oxygen ions are absorbed by the ceramic. To achieve the necessary oxygen content $YBa_2Cu_3O_{8.5+y}$

superconductor [27], the heated compounds must be slowly cooled in an oxygen atmosphere or be reheated in an oxygen atmosphere. The early experiments did not reveal the rare earth size effect since the variability of the oxygen contents(hole concentration) in the "123" series $REBa_2Cu_3O_{7-y}$ superconductors fabricated by Tarascon et al.[28] could mask changes in the superconducting transition temperature arising from a systematic change in the any variables in the host superconductor. Only when the hole concentration was kept constant, did the rare earth size effect reveal itself [29,30]. The T_c's reported by William and Tallon [29] are higher than reported by Tarascon [28] and Lin [30]. This is consistent with the idea that the specimens of William are optimally doped with the specimens of Lin are overdoped. By considering T_c to be a function of the hole concentration, there is a maximum in T_c at hole concentration of about 0.20-0.25 per Cu site, appears to be independent of how the hole are produced, e.g., dopant species, and strongly suggested that the hole concentration is the singularity most important factor in determining T_c [31].

2.2.2 Rare earth substitution

Shortly after the discovery of the $YBa_2Cu_3O_{7-y}$ superconductor, it was realized that the replacement of the yttrium ions by other rare earth ions would not destroy the "123" structure. It was somewhat surprising to find that, in most cases, the replacement of the yttrium ions by other rare earth ions did not lead to any appreciable changes in the transition temperatures [28,32]. Except for RE = La, Ce, Tb and Pr, all compounds $REBa_2Cu_3O_{7-y}$ were superconducting with T_c, above 90 K.

An explanation for the non formation of a superconducting phase by the four mentioned rare earths was that :

1. The La ions have the largest ionic radius of the rare earths and therefore the "123" structure would be distorted beyond recognition.

2. The Ce, Tb and Pr form into 4+ valence states.

However, some evidences have shown that the influence of rare earth element (RE) on T_c should not be ignored. To study the effects of RE substitutions in the $REBa_2Cu_3O_{7-y}$ superconductors, Williams and Tallon [29] fabricated a series of these superconductors having optimal hole concentration. Lin et al. [30] have fabricated a series of these superconductors which have the same oxygen content (6.97±0.03). Both groups observed that the T_c's increased with the size of the RE ions. Tang et al. [33] showed that the T_c of the RE-123 HTSCs would exhibit a quadratic ;dependence on the orthorhombic distortion (define as D = (b-a) / a , where a and b are the lattice parameters in the basal plane) of the ceramics. Since the changes in the T_c arising from the RE ion size effect are accompanied by changes in the orthorhombic distortion (the distortion within each HTSC series decreases with increasing RE ionic radii), the dependence of the T_c of the RE-123 HTSC on the radius of the RE ions may be due to the dependence of T_c on the orthorhombic distortion. It was seen that the T_c of the RE-123 HTSC decreased as the orthorhombic distortion increased.

2.2.3 Transition metal substitution

In $REBa_2Cu_{3-x}Zn_xO_{7-y}$ superconductors, substitution of Cu by other transition metals should produce a large change in the superconducting properties which, in turn, should shed light on the mechanisms responsible for the superconductivity. Several researchers chose to study the replacement of the Cu ions in RE-123 system and other HTSC's by other transition metal ions, both magnetic (Ni^{2+}, Fe^{3+} and Co^{3+}) and non

magnetic (Zn^{2+} and Al^{3+}) ions. They found that partial substitution of Cu decreases the critical temperature T_c for all transition metals. The suppression of the T_c by non magnetic Zn^{2+} was surprising since in conventional superconductors, non magnetic ion doping has negligible effects on the superconducting state (See Chapter 1).

Xiao et al.[23] have been able to fabricate the ceramics $YBa_2(Cu_{0.9}M_{0.1})O_{6+y}$ (M = Ti, Cr, Mn, Fe, Co and Ni). They found that the drop in T_c correlated with the size of the paramagnetic moments of the impurities except in the case of Zn. The drop in T_c caused by Zn substitution is due to the filling of the anti-bonding d band. Tarascon et al.[34] fabricated the system of $YBa_2Cu_{3-x}M_xO_{7-y}$ (M = Ni, Zn, Fe, Co and Al) and found both a depression of T_c for all dopants and the Fe, Co and Al doped phase became tetragonal with increasing x. Some of the results were also observed by Maeno et al.[35]. They show that for both Fe and Co doped materials, the oxygen content (y) changes as a function of doping content x, whereas no major changes are detected in the case of Zn or Ni. For trivalent ions (Co,Fe and Al), an orthorhombic-tetragonal structure transition takes place and simultaneously, the oxygen content (y) increases. This evidence show that Co, Fe, Al substitute mainly in the Cu(1) site. Whereas for divalent doping (Ni, Zn) both orthorhombic distortion and oxygen content are maintained, it is claimed that divalent Ni and Zn substitute for Cu(2) site. Ata-Allah et al.[36] presented experimental results dealing with the effect of RE ions on the superconducting T_c in the substituted $REBa_2Cu_{3-x}Zn_xO_{7-y}$ systems (R = Yb, Er, Y, Dy, Gd, Eu, Sm and Nd, and $0 \leq x \leq 0.1$). They found that substitution of Zn for Cu in these systems cause a rapid nearly linear suppression of the superconducting transition temperature T_c. All the $REBa_2Cu_{3-x}Zn_xO_{7-y}$ samples were essentially single phase and retain the orthorhombic structure in the range of substitution ($0 \leq x \leq 0.1$). The

reduction of T_c by Zn doping in the $REBa_2Cu_{3-x}Zn_xO_{7-y}$ was found to be strongly dependent on the ionic radius of the rare-earth element (RE). When the Zn doping concentration is kept constant, the suppression of T_c is increased by increasing the ionic radius of RE. Concerning the decrease rate of T_c, Peng et al.[37] found that the suppresion of T_c in the RE-123 by Zn^{2+} ion substitution is even greater than that due to Ni^{2+} ion substitution. System of $REBa_2Cu_{3-x}M_xO_7$ (RE = Sm, Dy; M = Fe, Ni, Zn) was studied by Sumana et al.[38]. They found that the T_c suppression rate for a given M ion depends on the ionic radius of the rare earth (RE) and is higher for larger rare earths.

As mentioned above, It can be concluded that the substituting elements can be divided into two groups (e.g. Al, Fe and Co) replacing Cu in the Cu(1)-O chain and causes a small changes in T_c ; elements of the other groups (e.g. Zn and Ni) mainly replace Cu in the Cu(2)-O planes and cause a significant degradation superconductivity. The results showed that the Cu(2)-O planes play a more important role than the Cu(1)-O chains in the RE-123 system.

2.3 Aim to Study

After discovery of 90 K in $YBa_2Cu_3O_7$, this opened a wide range of technological application. The evolution of the field, both experimental and theoretical has been very rapid. There are many different results from experiments and may be explained by the following reasons ; (i) a change in the oxygen stoichiometry or hole concentration (ii) the orthorhombic to tetragonal transformation or orthorhombic distortion (iii) the

nature of the impurity doping. However, several of the reasons are interrelated. In the present study, we have carried out systematic substitutional studies on $REBa_2Cu_{3-x}Zn_xO_{7-y}$ (RE = Er, Y, Ho, Dy, Gd and Sm, and $0 \leq x \leq 0.012$) with the following objectives: determine the effect of non magnetic ion substitution and the ionic radius of the rare earth ion on the T_c suppression rates in the $REBa_2Cu_{3-x}Zn_xO_{7-y}$ system which show that there is no discernable change in the crystal structure with Zn^{2+} ion doping as observed by powder X-ray diffraction.

2.4 Method of Research

The method starts the following procedures :

(1) Calculate chemical compounds by stochiometric amount of each materials.

(2) Preparation of ceramic samples by using the conventional solid state reaction method.

(3) Sintering samples in the furnance.

(4) Characterization the samples by

- powder X-ray diffraction with Cu K_α radiation to determine that the lattice parameters remained invariant with Zn substitution.
- iodometric titration to determine the copper valency
- four probe method to measure the resistivity (critical temperature)

CHAPTER III

EXPERIMENTAL METHODS

3.1 Instrumentation

The investigation was made possible through the use of the following equipment:

- Powder X-ray Diffractometer (Philips TW 1830)
- Four-probe Apparatus
- Iodometric Titration Apparatus
- Analytical Balance (Mettler AJ 150)
- Hydraulic Press and Die Set
- Furnace (Lindberg model 59256 – P – COM)
- Furnace (Lenton Model EHF 18/5)
- Alumina Crucibles
- Agate Mortar
- Dessicator

3.2 Chemicals

All chemicals used were of analytical, high purity grade from Fluka Chemika

- Erbium Oxide (Er_2O_3 99.9 %)
- Yttrium Oxide (Y_2O_3 > 99.9 %)
- Holmium Oxide (Ho_2O_3 > 99.9 %)
- Dysprosium Oxide (Dy_2O_3 > 99.9 %)
- Gadolinium Oxide (Gd_2O_3 > 99.9 %)
- Samarium Oxide (Sm_2O_3 > 99.9 %)
- Barium Carbonate ($BaCO_3$ > 99 %)
- Copper Oxide (CuO > 99.9 %)
- Zinc Oxide (ZnO > 99 %)

3.3 Calculation the Stoichiometric Amount of Chemical Compound

If one wants to fabricated $YBa_2Cu_{3-x}Zn_xO_{7-y}$ with x = 0.002 from starting chemicals : Y_2O_3 = 225.81 amu., Y = 88.91 amu.

$BaCO_3$ = 197.37 amu., Ba = 137.34 amu.

CuO = 79.54 amu., Cu = 63.55 amu.

ZnO = 81.37 amu., Zn = 65.38 amu.

Let M_{total} = gram equivalents of cations in one mole

and f = fraction of mole needed = 30 grams / M_{total}

M_{total} = 88.91+2(137.34)+2.998(63.55)+0.002(65.38) = 554.228

f = 30 / 554.228 = 0.0541

Then $fM_Y = 0.0541 \times 88.91 = 4.8098$

$2\ fM_{Ba} = 2 \times 0.0541 \times 137.34 = 14.8602$

$2.998\ fM_{Cu} = 2.998 \times 0.0541 \times 63.55 = 10.3066$

$0.002\ fM_{Zn} = 0.002 \times 0.0541 \times 65.38 = 0.8035$

And fraction of Y in Y_2O_3 is $2M_Y / Y_2O_3 = (2 \times 88.91) / 225.81 = 0.7874$

fraction of Ba in $BaCO_3$ is $M_{Ba} / BaCO_3 = 137.34 / 197.37 = 0.6908$

fraction of Cu in CuO is $M_{Cu} / CuO = 63.55 / 79.54 = 0.7989$

fraction of Zn in ZnO is $M_{Zn} / ZnO = 65.38 / 81.37 = 0.8035$

Then the weight of Y_2O_3 needed to make 30 grams is

fM_Y / fraction of Y in Y_2O_3 = 4.8098 / 0.7874 = 6.1084 grams

The weight of $BaCO_3$ needed to make 30 grams is

$2\ fM_{Ba}$ / fraction of Ba in $BaCO_3$ = 14.8602 / 0.6908 = 21.3570 grams

The weight of CuO needed to make 30 grams is

$2.998\ fM_{Cu}$ / fraction of Cu in CuO = 10.3066 / 0.7898 = 12.9010 grams

The weight of ZnO needed to make 30 grams is

$0.002\ fM_{Zn}$ / fraction of Zn in ZnO = 0.0071 / 0.8035 = 0.0088 grams

3.4 Preparation of Ceramic Samples

A total of 42 compositions of $REBa_2Cu_{3-x}Zn_xO_{7-y}$ (RE = Er, Y, Ho, Dy, Gd and Sm) with $0 \leq x \leq 0.012$ (in step of 0.002) were synthesized using the conventional solid state reaction method. Stoichiometric amounts of raw materials (RE_2O_3, $BaCO_3$, CuO and ZnO with high purity) were carefully weighed and mixed in a agate mortar at least half an hour for each sample. The mixed powders placed in alumina

crucibles, were calcined at 910 °C for 24 hours. The powders were heated to desired temperature at the rate of 4 °C / min in a Linberg furnace, and cooling by the rate of 10 °C / min to room temperature with in the furnace. The purpose of the prefiring is to get solid state reaction to occur. After this process, calcined powder was obtained. Figure 3.1 shows a typical program for calcining at 910 °C for 24 hours.

3.5 Sintering Processes

The calcined powders were then reground and pressed into pellets of approximately of 1 cm in diameter and about 2 mm in thickness using a stainless steel die set under uniaxial pressure of 2000 psi . This gave several pellets of each composition which were then sintered at 930 °C in the air for 24 hours. The heating rate was again 4 °C / min by Lenton furnace. After this they were cooled to room temperature in a flowing oxygen atmosphere at the rate of 1 °C / min. The proper hole concentrations were achieved during the slow cooling down cycle. During the sintering process, the crystallization takes place and black-pellet samples were formed. A typical program of this sintering process was shown in Figure 3.2.

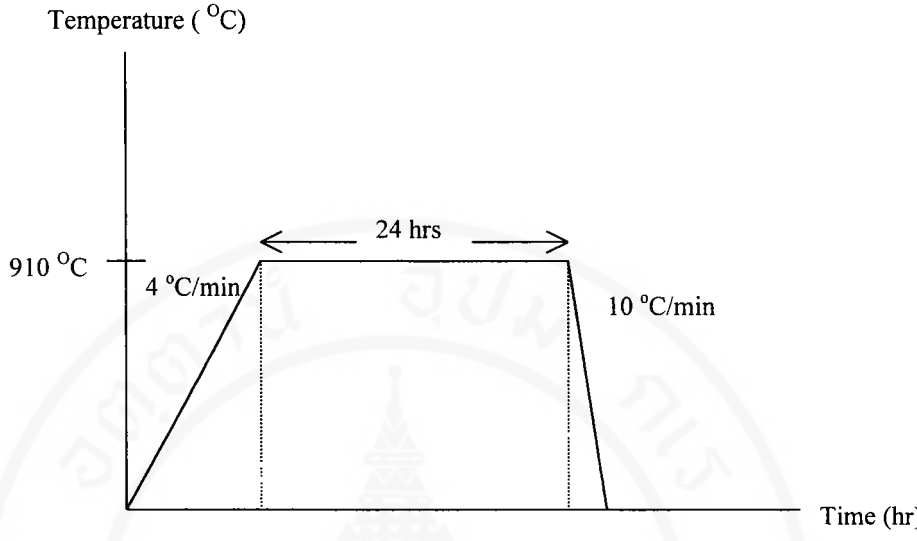

Figure 3.1 Typical program showing heating steps for calcination

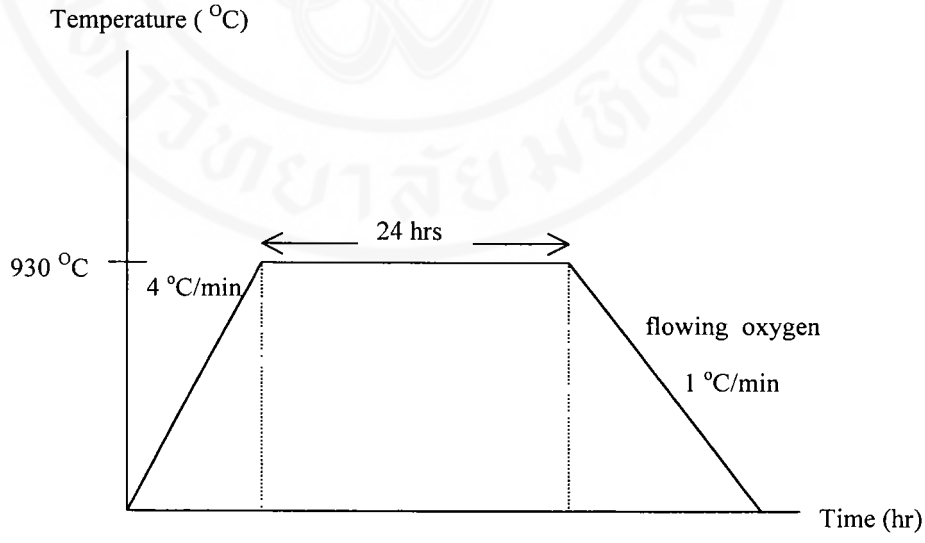

Figure 3.2 Typical program showing heating steps for sintering

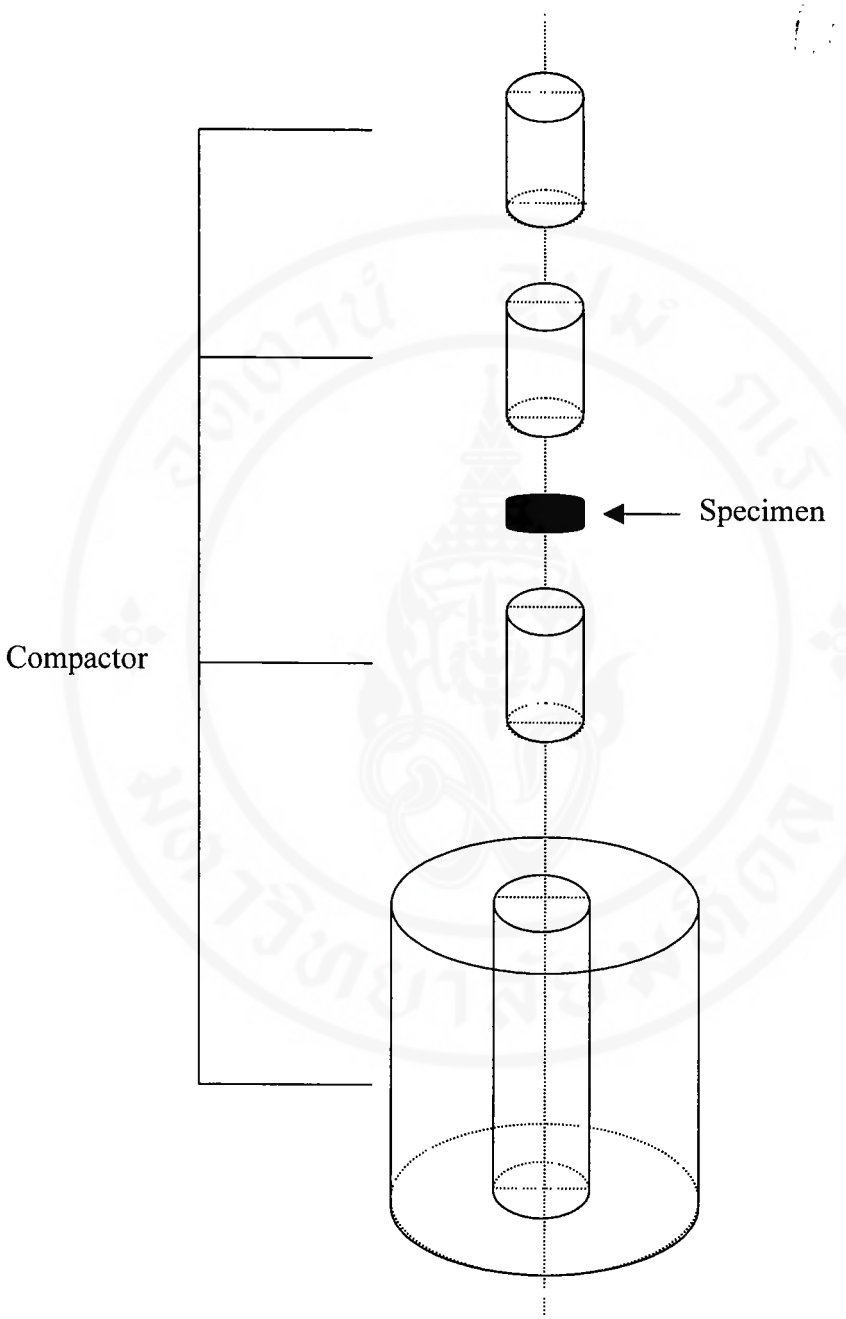

Figure 3.3 The compactor unit for pressed pellet.

3.6 Characterization

3.6.1 Powder X-ray diffraction (XRD)

The sintered samples were analyzed qualitatively by a powder X-ray diffractometer using CuK_α radiation. It was operated with a rotating target X-ray diffractometer.

From Bragg's law

$$2d_{hkl}\sin\theta = n\lambda$$

where d_{hkl} is plane spacing

θ is diffraction angle

n is order of diffraction (1, 2, 3, ...)

λ is X-ray wavelength

and h,k,l are Miller indices

Then the relation between d-spacing with lattice parameters of orthorhombic unit cell was calculated from

$$\frac{1}{d_{hkl}^2} = \frac{h^2}{a^2} + \frac{k^2}{b^2} + \frac{l^2}{c^2}$$

The procedure is done as follows :

1. Grinding sample into fine powder and putting into the glass tray.

2. Placing the tray into powder X-ray diffractometer and radiating with CuK_α having wavelength 1.54178 Å. The reflections were recorded over a range of 2θ from 10 ° to 80 °.

3. From each diffraction pattern, the values of 2θ and corresponding d-values

were calculated.

4. Comparing these with d-values reference,identifying the planes (hkl).

5. Calculating the lattice parameters by input θ, diffraction planes(hkl) and peak intensity into IBMCENE program.

3.6.2 Iodometric titration method

The method gave an average oxidation state of the copper which was done by dissolving the sample in an acidified solution of KI followed by back titration. The copper valency of sample could generally be determined by two sets of experiments [39].

Experiment A

A sample of 150-200 mg was accurately weighed and dissolved in 10 ml of 1.0 M HCl in titration beaker. The solution was then gently boiled for 10 minutes to ensure that all Cu^{3+} ions were converted to Cu^{2+}. This whole process was done in a fume hood after which was left to cool down to room temperature. A buret and a gas inlet were inserted through two holes in a rubber stopper over the beaker. With N_2 starting to flow to flush out all oxygen, 10 ml of distilled water containing 1.0-1.5 grams of KI was added and titrated as above with magnetic stirring by 0.03 M $Na_2S_2O_3$ solution (standardized by standard copper solution) with a few drops of starch. In experiment A, the sample was first dissolved in dilute HCl and Cu^{3+} was rapidly reduced to Cu^{2+} as a result :

$$2\ Cu^{3+}(aq) + H_2O\ (l) \rightarrow 2\ Cu^{2+}(aq) + 1/2\ O_2(g) + 2H^+(aq)$$

The solution is then treated with iodide to get

$$Cu^{2+}(aq) + 2I^{-}(aq) \rightarrow CuI\,(s) + 1/2\,I_2\,(aq)$$

and titration of the liberated iodine with standard thiosulfate solution

$$I_2\,(aq) + 2S_2O_3^{2-}(aq) \rightarrow 2I^{-}(aq) + S_4O_6^{2-}(aq)$$

The number of moles of thiosulfate used to titrate the iodine is equal to the number of moles of Cu ions (both the divalent and trivalent species) in experiment A.

Experiment B

A sample of 150-200 mg was accurately weighed and dissolved in 10 ml of a mixture of 1.0 M HCl / 0.07 KI in titration beaker. A buret and a gas inlet were inserted through two holes in a rubber stopper over the beaker. With N_2 starting to flow to flush out oxygen, a magnetic bar was stirred for 1 minute. Then distilled water was added 10 ml and titrated by 0.03 M $Na_2S_2O_3$ the same as experiment A. The differrent Cu ions react as follows :

$$Cu^{3+}(aq) + 3I^{-}(aq) \rightarrow CuI\,(s) + I_2\,(aq)$$

$$Cu^{2+}(aq) + 2I^{-}(aq) \rightarrow CuI\,(s) + 1/2\,I_2\,(aq)$$

The number of moles of thiosulfate needed to titrate the liberated I_2 would now correspond to 1 mol Cu^{2+} and 2 mol Cu^{3+}. The difference between the results of the two experiments of the titration is the content of the Cu^{3+} in the specimens.

3.6.3 Four-probe method

The resistance as a function of temperature was measured on a pellet by standard four-probe technique. From Ohm's law

$$R = V / I$$

where R resistivity, V is voltage drop between a pair of probes, and I is current.

The value of voltage drop across the surface of sample varied as the temperature of the sample was lowered to liquid nitrogen, accordingly due to thermocouple was the monitor the change in temperature in order to find to

1. Putting four spots of indium solder on the one side of the pellet while the thermocouple junction was placed in contact with the other side of the pellet as shown in Figure 3.4

2. Connecting two points of the probe to a current source and the other two points to a millivoltmeter while another millivoltmeter was attached to two ends of the thermocouple.

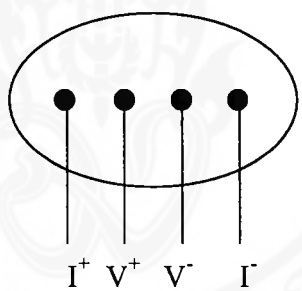

Figure 3.4 Connection of sample and probe

3. Passing constant current approximately 1 mA to the probe.

4. Turning on computer, which hooks up to two millivoltmeters, and calling for the program.

5. Dipping a probe into liquid nitrogen until the millivoltmeter to probe reads zero.

6. Lifting the probe over liquid nitrogen, followed by running the program.

7. The computer records all the values of emf of the thermocouple and the voltage drop across the pellet surface.

8. Calibrating the thermocouple with emf readings at liquid nitrogen and room temperature.

9. Converting the emf readings to temperature by using the table given by a thermocouple manufacturer.

10. Plotting temperature readings against corresponding voltage drops and locating T_c.

3.7 Flow Diagram of Experimental Procedures

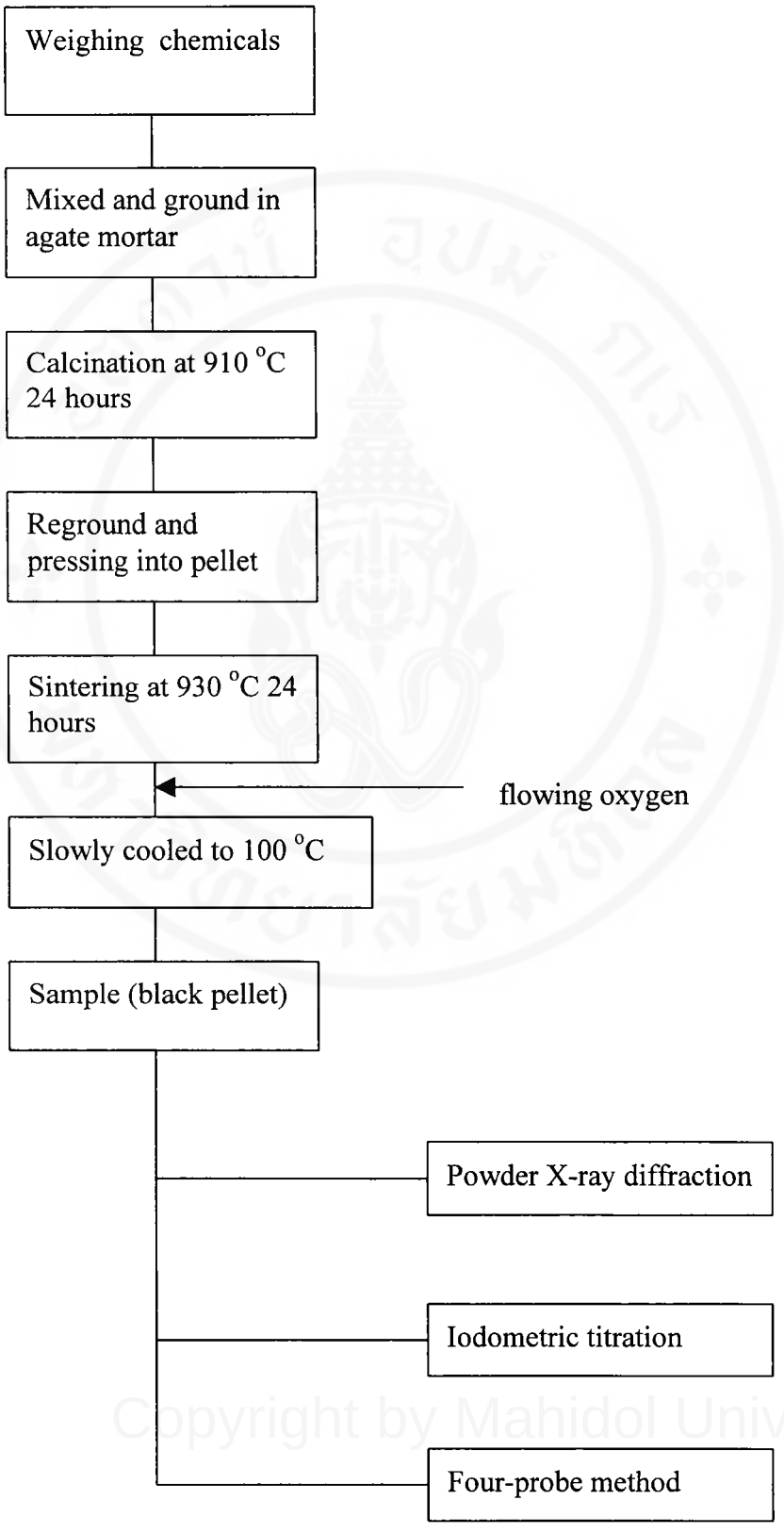

CHAPTER IV

RESULTS

4.1 Copper Valency

The copper valency in the sample is determined by the iodometric titration method which gives the average oxidation state of the copper ions. We determined the copper valency of all specimen fabricated. Since the optimal T_c occurs at the same valency for all RE-123, we have only carried out measurements of T_c having nearly identical valencies. In Table 4.1-4.6 and Figure 4.1 show the copper valency of the subset of pellets on which further experiments were performed on. From the results, it was found that the copper valency is almost independently of substitution of Zn for Cu in these systems and are not caused by the change of the hole concentration [38].

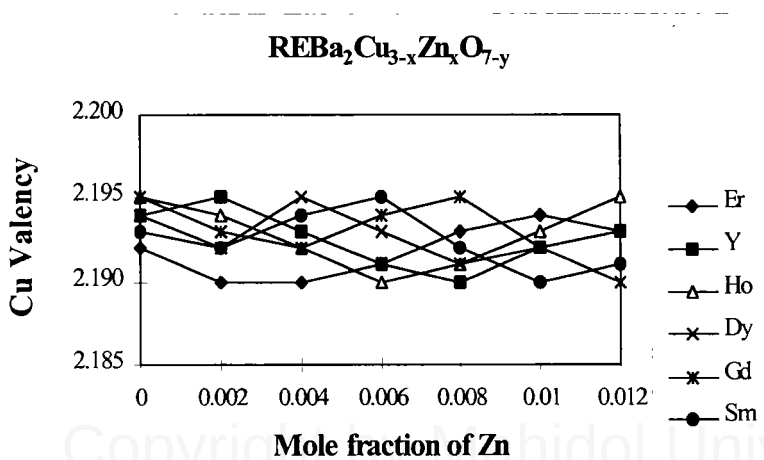

Figure 4.1 Variation of copper valency with mole fraction of Zn

Table 4.1 Lattice parameters, orthorhombic distortion (D), copper valency and T_c of $ErBa_2Cu_{3-x}Zn_xO_{7-y}$

Mole fraction of Zn	a (Å)	b (Å)	$Dx10^{-2}$	Cu valency	T_c (K)
x = 0.000	3.8140	3.8832	1.969	2.192	91.37
x = 0.002	3.8148	3.8842	1.817	2.190	88.98
x = 0.004	3.8137	3.8834	1.828	2.190	82.86
x = 0.006	3.8138	3.8837	1.833	2.191	80.02
x = 0.008	3.8143	3.8840	1.829	2.193	79.84
x = 0.010	3.8139	3.8837	1.831	2.194	79.96
x = 0.012	3.8197	3.8859	1.822	2.193	79.78
		Average distortion	1.847		

Table 4.2 Lattice parameters, orthorhombic distortion (D), copper valency and T_c of $YBa_2Cu_{3-x}Zn_xO_{7-y}$

Mole fraction of Zn	a (Å)	b (Å)	$Dx10^{-2}$	Cu valency	T_c (K)
x = 0.000	3.8192	3.8851	1.724	2.194	91.82
x = 0.002	3.8181	3.8850	1.754	2.195	89.04
x = 0.004	3.8179	3.8848	1.754	2.193	84.26
x = 0.006	3.8180	3.8848	1.750	2.191	82.56
x = 0.008	3.8184	3.8852	1.750	2.190	80.26
x = 0.010	3.8177	3.8841	1.740	2.192	80.15
x = 0.012	3.8176	3.8847	1.757	2.193	79.84
		Average distortion	1.747		

Table 4.3 Lattice parameters, orthorhombic distortion (D), copper valency and T_c of $HoBa_2Cu_{3-x}Zn_xO_{7-y}$

Mole fraction of Zn	a (Å)	b (Å)	$Dx10^{-2}$	Cu valency	T_c (K)
x = 0.000	3.8184	3.8856	1.760	2.195	92.04
x = 0.002	3.8172	3.8862	1.807	2.194	89.04
x = 0.004	3.8187	3.8859	1.761	2.192	85.15
x = 0.006	3.8171	3.8856	1.794	2.190	82.68
x = 0.008	3.8172	3.8859	1.799	2.191	80.80
x = 0.010	3.8175	3.8859	1.790	2.193	80.09
x = 0.012	3.8176	3.8863	1.800	2.195	79.84
		Average distortion	1.787		

Table 4.4 Lattice parameters, orthorhombic distortion (D), copper valency and T_c of $DyBa_2Cu_{3-x}Zn_xO_{7-y}$

Mole fraction of Zn	a (Å)	b (Å)	$Dx10^{-2}$	Cu valency	T_c (K)
x = 0.000	3.8254	3.8879	1.634	2.194	92.47
x = 0.002	3.8271	3.8882	1.597	2.192	89.15
x = 0.004	3.8267	3.8871	1.580	2.195	85.26
x = 0.006	3.8263	3.8879	1.611	2.193	82.97
x = 0.008	3.8268	3.8883	1.605	2.191	81.03
x = 0.010	3.8258	3.8875	1.612	2.192	80.15
x = 0.012	3.8269	3.8870	1.570	2.190	79.90
		Average Distortion	1.601		

Table 4.5 Lattice parameters, orthorhombic distortion (D), copper valency and T_c of $GdBa_2Cu_{3-x}Zn_xO_{7-y}$

Mole fraction of Zn	a (Å)	b (Å)	$Dx10^{-2}$	Cu valency	T_c (K)
x = 0.000	3.8364	3.8916	1.440	2.195	93.10
x = 0.002	3.8363	3.8917	1.443	2.193	89.27
x = 0.004	3.8373	3.8925	1.438	2.192	85.26
x = 0.006	3.8366	3.8921	1.445	2.194	83.09
x = 0.008	3.8385	3.8931	1.422	2.195	81.40
x = 0.010	3.8377	3.8932	1.447	2.192	80.15
x = 0.012	3.8380	3.8932	1.439	2.190	79.96
		Average distortion	1.439		

Table 4.6 Lattice parameters, orthorhombic distortion (D), copper valency and T_c of $SmBa_2Cu_{3-x}Zn_xO_{7-y}$

Mole fraction of Zn	a (Å)	b (Å)	$Dx10^{-2}$	Cu valency	T_c (K)
x = 0.000	3.7977	3.8373	1.043	2.193	93.26
x = 0.002	3.7990	3.8376	1.000	2.192	89.43
x = 0.004	3.7975	3.8367	1.033	2.194	85.38
x = 0.006	3.7972	3.8373	1.055	2.195	83.15
x = 0.008	3.7981	3.8383	1.056	2.192	81.52
x = 0.010	3.7981	3.8376	1.026	2.190	80.62
x = 0.012	3.7977	3.8369	1.031	2.191	79.96
		Average Distortion	1.035		

4.2 Results From Powder X-Ray Diffraction

All compositions of the system $REBa_2Cu_{3-x}Zn_xO_{7-y}$ (RE = Er, Y, Ho, Dy, Gd and Sm, $0 \leq x \leq 0.012$) are black in color and stable under normal atmospheric conditions. Powder X-ray diffractions were performed at room temperature by using a Philips TW 1830 with Cu K_α radiation were performed. The X-ray diffraction peaks of $GdBa_2Cu_{3-x}Zn_xO_{7-y}$ are shown in Figure 4.2 as an example of the $REBa_2Cu_{3-x}Zn_xO_{7-y}$. The peak positions for both the substituted and pure copper 1-2-3 compounds coincided very well for all compositions. This indicated that the sample were of the 1:2:3 phase and the orthorhombic structure remained unchanged for all Zn concentration in $REBa_2Cu_{3-x}Zn_xO_{7-y}$.

From X-ray pattern, using the IBMCENE program, we calculated the lattice parameters. The values of the lattice parameters a and b for the specimens are list in Table 4.1 - 4.6. There are small changes in these parameters as the Zn^{2+} ions are added. The results indicate that substitution of Zn for Cu in these systems maintain the orthorhombic structure for the range of substitution [28,36].

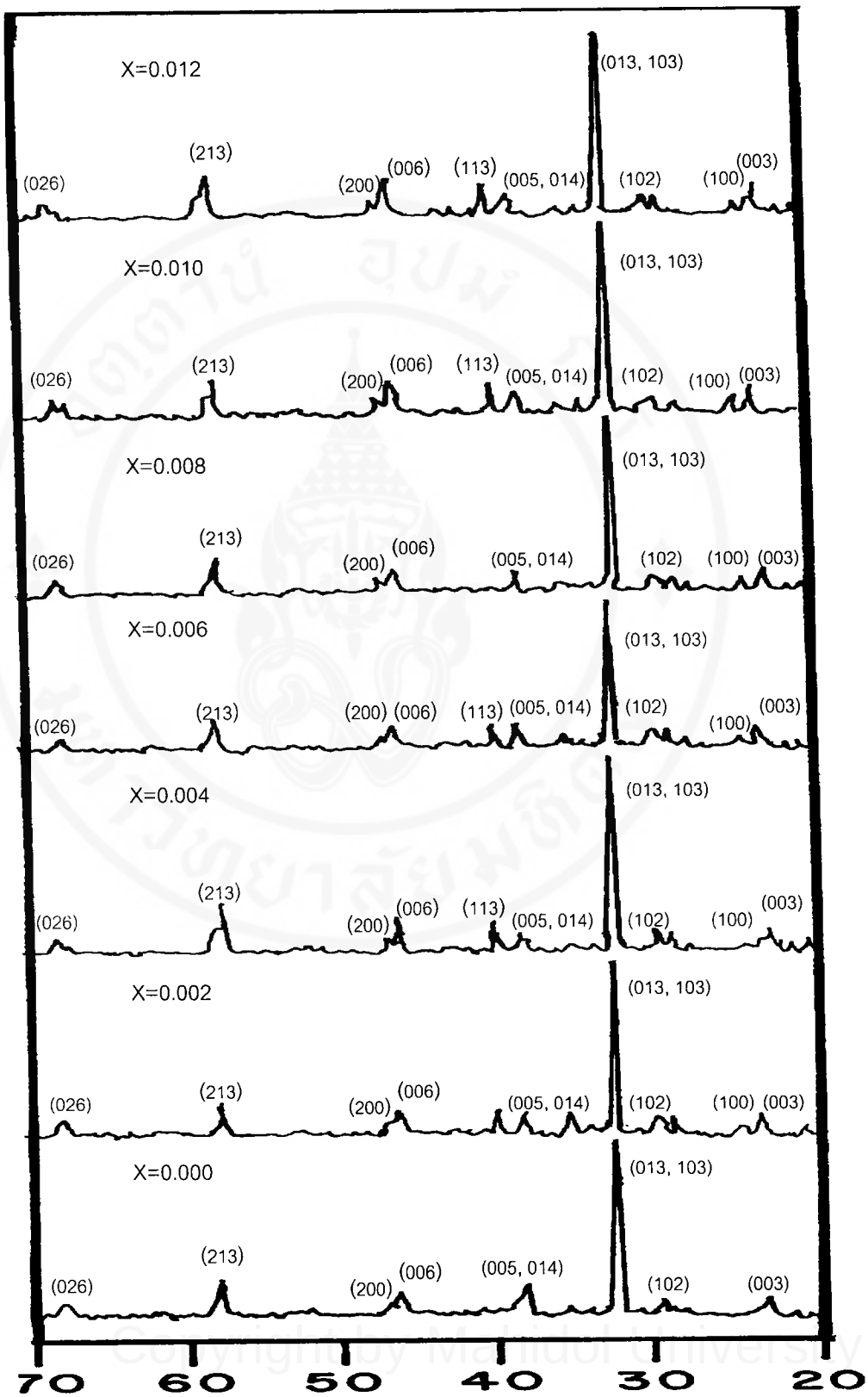

Figure 4.2 X-ray diffraction pattern of $GdBa_2Cu_{3-x}Zn_xO_{7-y}$

The orthorhombic distortion (defined as D = (b-a) / a with a and b being the lattice parameters in the basal plane) of these systems were calculated and their values were shown in Table 4.1 – 4.6. The orthorhombic distortion is clearly related to the rare earth ion size as shown in Figure 4.3. It is found that the orthorhombic distortion decrease as the rare earth ion size increases. Furthermore, they were found to be independent of Zn substitution [42].

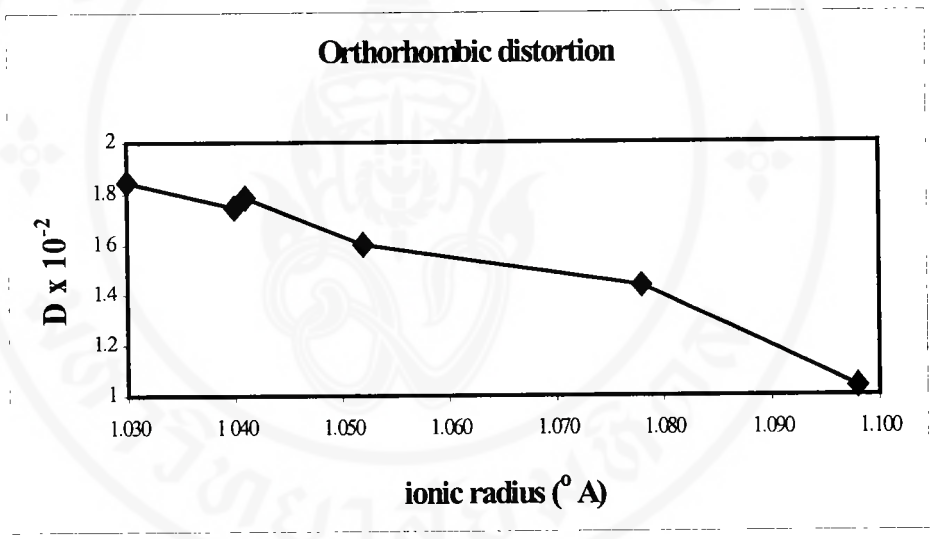

Figure 4.3 Variation of orthorhombic distortion with ionic radius of rare earth in $REBa_2Cu_{3-x}Zn_xO_{7-y}$ (RE = Er, Y, Ho ,Dy, Gd and Sm)

4.3 Critical Temperature

The critical temperatures were measured using the standard four-probe method. The critical temperature T_c is defined as the temperature at which the resistance extrapolates to zero. The data of critical temperature for the $REBa_2Cu_{3-x}Zn_xO_{7-y}$ system with Zn concentrations x = 0.000, 0.002, 0.004, 0.006, 0.008, 0.010 and 0.012 are also reported in Table 4.1 –4.6 and shown in Figure 4.4 as an example of the $ErBa_2Cu_{3-x}Zn_xO_{7-y}$. The temperature dependence of the resistivity for these systems is shown in Figure 4.5-4.10. It is indicated that substitution Zn for Cu, the T_c decreases as the Zn concentration increases in each RE-123 system. In $REBa_2Cu_{3-x}Zn_xO_{7-y}$ system at constant Zn concentration, T_c is observed to increase with the size of the rare earth ion. It is found that the rate of suppression of T_c due to Zn^{2+} doping in the different RE-123 system is higher for larger rare earths [36].

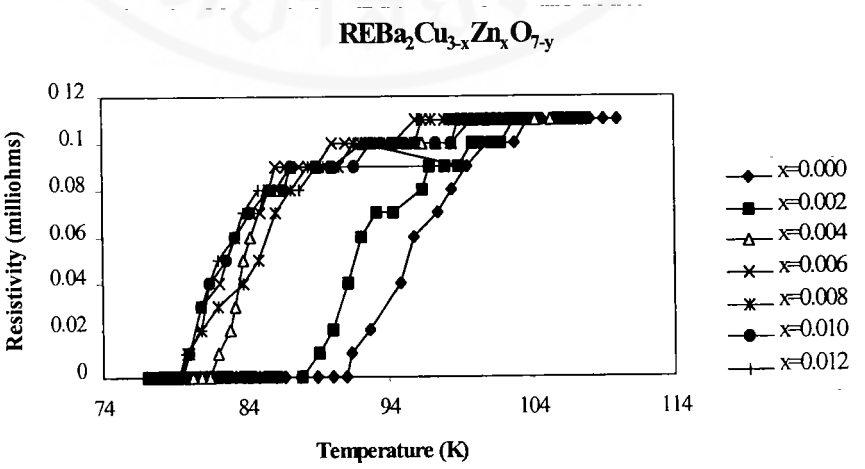

Figure 4.4 Temperature dependence of the resistivity of $ErBa_2Cu_{3-x}Zn_xO_{7-y}$

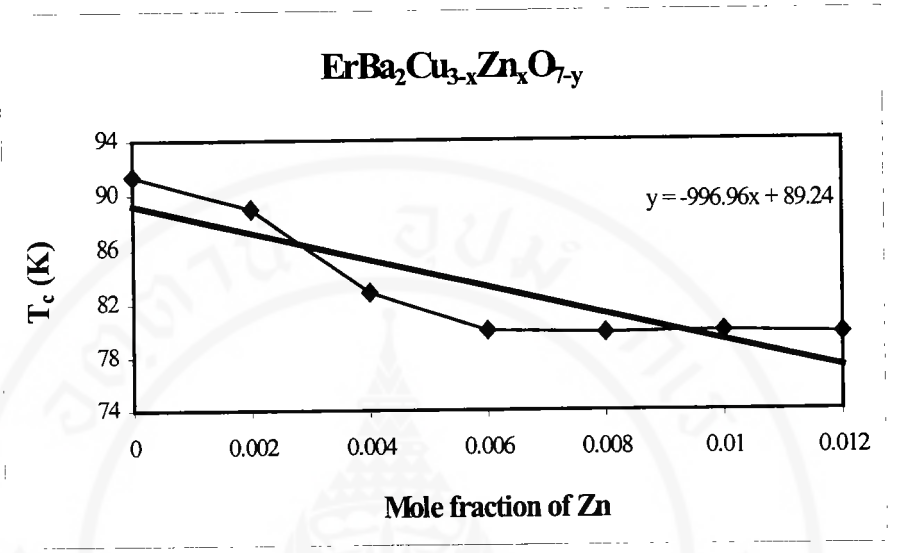

Figure 4.5 Depression T_c of $ErBa_2Cu_{3-x}Zn_xO_{7-y}$ with mole fraction of Zn

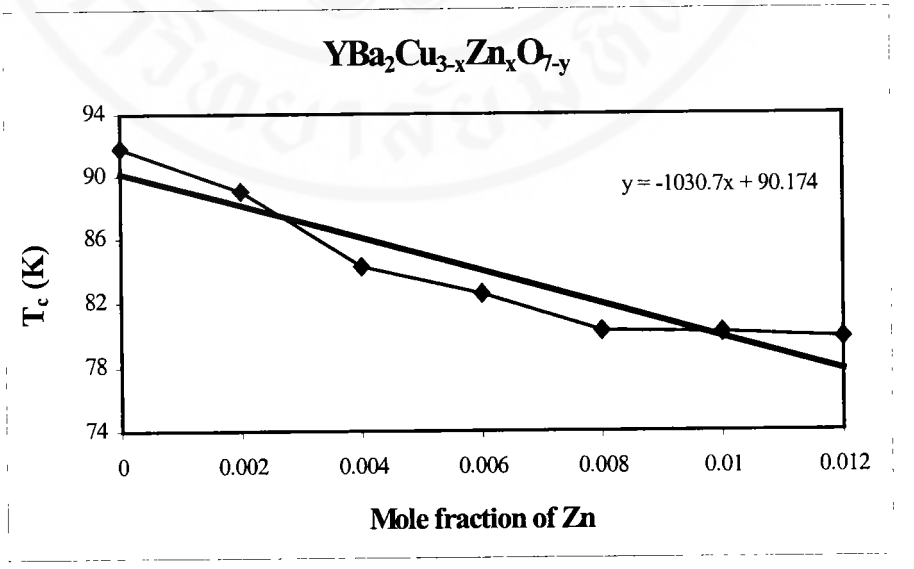

Figure 4.6 Depression T_c of $YBa_2Cu_{3-x}Zn_xO_{7-y}$ with mole fraction of Zn

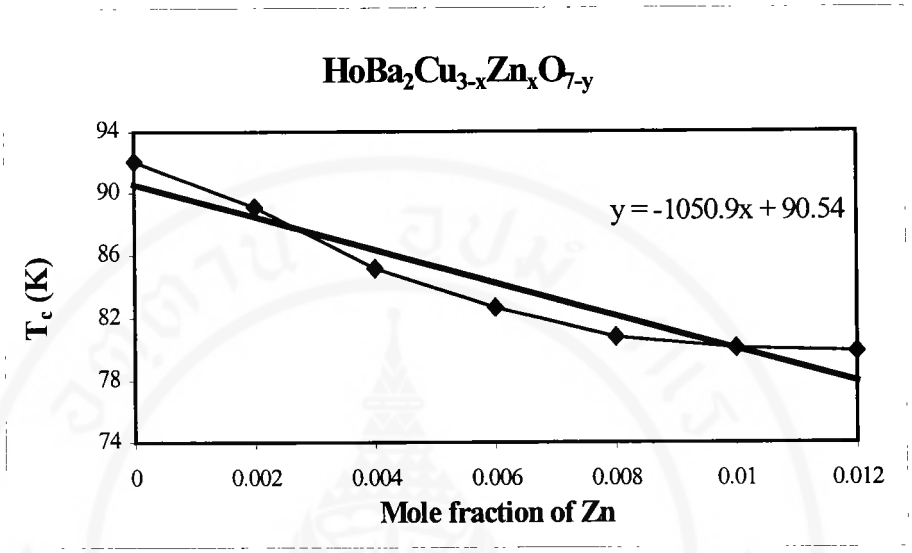

Figure 4.7 Depression T_c of $HoBa_2Cu_{3-x}Zn_xO_{7-y}$ with mole fraction of Zn

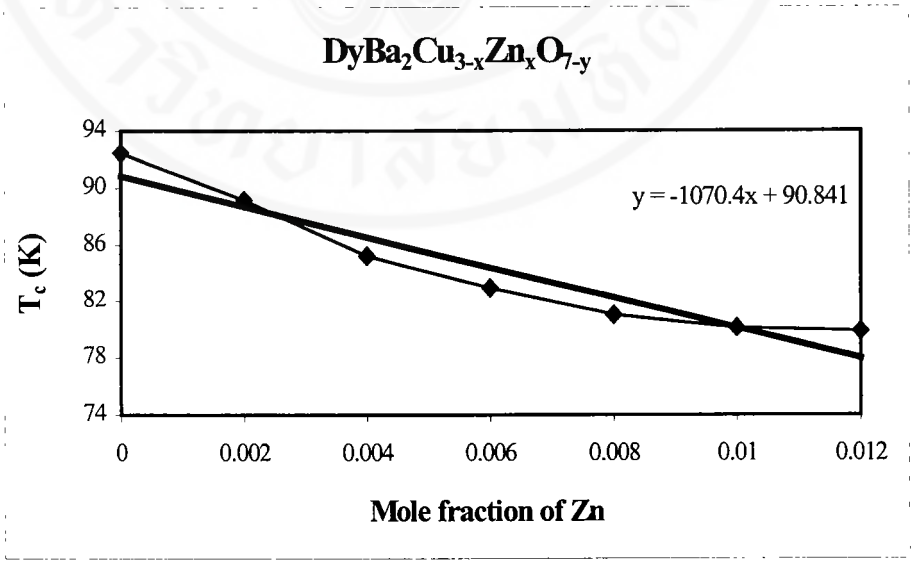

Figure 4.8 Depression T_c of $DyBa_2Cu_{3-x}Zn_xO_{7-y}$ with mole fraction of Zn

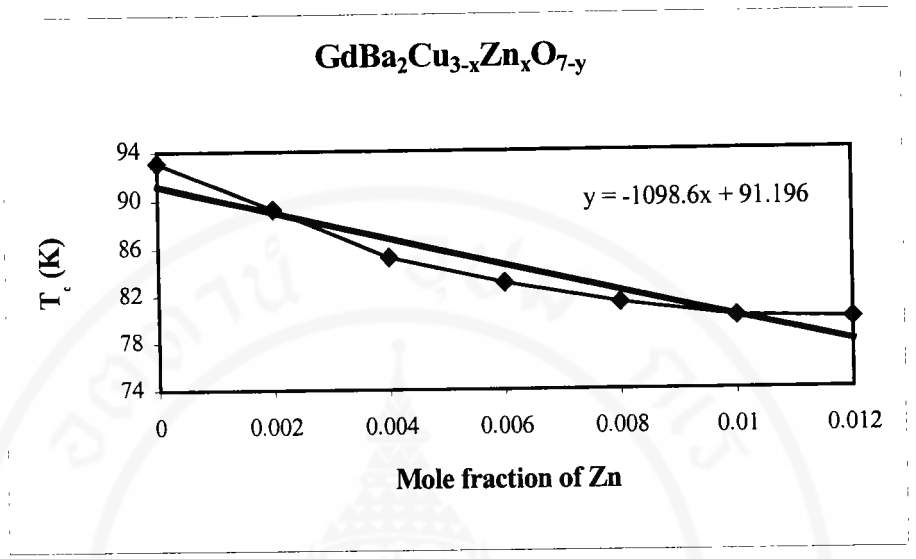

Figure 4.9 Depression T_c of $GdBa_2Cu_{3-x}Zn_xO_{7-y}$ with mole fraction of Zn

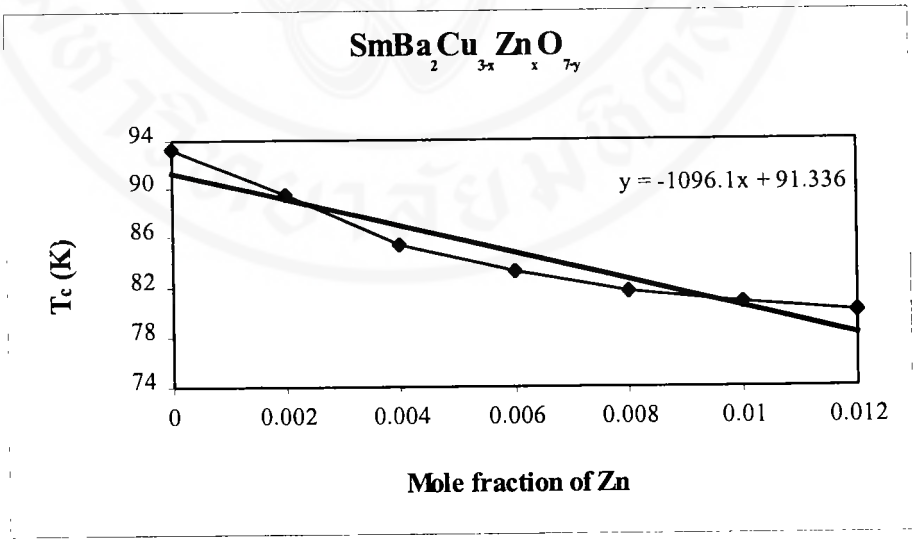

Figure 4.10 Depression T_c of $SmBa_2Cu_{3-x}Zn_xO_{7-y}$ with mole fraction of Zn

CHAPTER V

DISCUSSION AND CONCLUSION

5.1 Discussion

As it had already earlier pointed out, the pair condensation in both conventional and unconventional superconductor is due to the existence of attractive interaction between electrons of opposite momentum and spin (Cooper pair). The observation of the isotope effect in conventional superconductors pointed to the role of phonons in these phenomena. This leads to the Bardeen-Cooper-Schrieffer (BCS) theory of superconductivity.

The observation of a nearly four clover-shaped of the order parameter (OP) in the high temperature superconductors pointed to the fact that the mechanism responsible for pair condensation in the high temperature superconductor was not the electron-phonon interaction since that interaction would produce a symmetrically shaped order parameter.

One of the bosons existing in the perovskite copper oxide structure is the local spin fluctuations (LSF). The spin fluctuations arise due to the random hopping of holes (or electrons) from a $Cu^{2+} \rightarrow Cu^{3+}$. The local spin fluctuations would arise from the quantization of these random hopping occurring on a square array (i.e. on the 2D CuO_2 layer), the resulting local spin fluctuation will exhibit the symmetry of the CuO_2 layer.

The exchange of bosons having this symmetry as the mechanism responsible for the formation of the order parameter, gives rise to the d-wave theory of superconductivity.

In the presence of orthorhombic distortion of the CuO_2 layer, the symmetry characterization of local spin fluctuations will also change. This gives rise to the (d+s) wave theory of high temperature superconductors. The distortion of symmetry of the local spin fluctuations spectrum can be correlated to the orthorhombic distortion [40]. In the paper, it was shown that [41]

$$T_c = T_{c0}\left\{1 - \alpha^2(D)\left(\frac{V_{ani}}{g_{sf}\chi J}\right)^2 \frac{1+\chi J}{g_{sf}\chi J - \alpha(D)V_{iso}}\right\} \qquad (5.1)$$

with T_{c0} is the temperature which absence of the orthorhombic distortion , g_{sf} is the strength of the coupling between the carriers and the spin fluctuations; χ is the spin susceptibility function which describes the spin fluctuations responsible for the pair condensation in the plane; J is the weight of the spectral density representation of the susceptibility function at the magnetic Einstein frequency; $\alpha(D)$ is a parameter which depends on the orthorhombic distortion and which vanishes in the absence of the orthorhombic distortion; V_{ani} is a nonseparable anisotropic pairing potential and where V_{iso} is an isotropic potential which leads to a s-wave component to the order parameter.

5.2 Conclusion

The above section is based on the assumption that $\alpha(D)$ is the controlling parameter. According to chapter II, T_c also depends on the copper valency and may be the distance between layers. Since we have only looked at specimens having nearly identical copper valencies and interlayer distances. The equation (5.1) should be able to describe our results. As orthorhombic distortion (D) decreases when the ionic radius increase, i.e.,

$$D(Er) > D(Y) > D(Ho) > D(Dy) > D(Gd) > D(Sm) \qquad (5.2)$$

(since $\alpha(D)$ is proportional to D (see Ref. 32)), Equation (5.1) would predict T_c increasing, i.e., T_c (Er) < T_c (Y) < T_c (Ho) < T_c (Dy) < T_c (Gd) < T_c (Sm). This is indeed observed according to Lin et al.[30] the T_c's are 91.5 K, 91.7 K, 93.1 K and 94.4 K in the order noted. Taking the values for the rates of depression due to Zn substitution given in Ref. 39, we find that the slopes obey in general the relation

$$\left.\frac{dT_c}{dx}\right|_{\text{larger RE radius}} > \left.\frac{dT_c}{dx}\right|_{\text{smaller RE radius}} \qquad (5.3)$$

Using the form of dT_c/dx given by

$$\left.\frac{dT_c}{dx}\right|_{n_{imp}\to 0} = -\frac{\pi}{4}C\left(\sigma_n' + \frac{4T_{c0}}{\pi C_{cr}}\chi_{c0}\right)\{1-\alpha(D)B\} \qquad (5.4)$$

where

$$C^{-1} = \left\{1 + \alpha(D)\frac{V_{iso}}{g_{sf}\chi J} - \alpha^2(D)\frac{V_{iso}g_{sf}\chi J - V_{ani}^2}{g_{sf}\chi J Z_0}\chi_{c0}\right\} \qquad (5.5)$$

and

with X_{co} being the value of X_c at the transition temperature of the host "RE-123" HTSC. We have

$$\left(\sigma_n' + \frac{4X_{c0}(L)T_{c0}(L)}{\pi C_{cr}}\right)\left(\frac{1-\alpha(L)B}{1+\alpha(L)B'}\right) > \left(\sigma_n' + \frac{4X_{c0}(S)T_{c0}(S)}{\pi C_{cr}}\right)\left(\frac{1-\alpha(S)B}{1+\alpha(S)B'}\right) \tag{5.7}$$

and where B' are the terms in C^{-1} which are proportional to the orthorhombic distortion parameter $\alpha(D)$ and $L(S)$ denoted that the quantity (or parameter) is for the larger (smaller) RE ionic radii. If $\sigma_n' \rangle\rangle 4X_{c0}T_{c0}/\pi C_{cr}$, then the inequality given by equation (5.7) becomes

$$\frac{1-\alpha(L)\,B}{1+\alpha(L)\,B'} > \frac{1-\alpha(S)\,B}{1+\alpha(S)\,B'} \tag{5.8}$$

which would be satisfied when $\alpha(S) > \alpha(L)$. Looking at the inequalities given by equation (5.2), we indeed see that this in equality is true. For the other condition $\sigma_n' \langle\langle 4X_{c0}T_{c0}/\pi C_{cr}$, the inequality, equation (5.3), would be assured if $_{c0}(L) > _{c0}(S)$ and $\alpha(S) > \alpha(L)$. These two inequalities are satisfied by the "RE-123" HTSC's. We thus see that the predictions based on a (d+s)-wave model of the "RE-123" HTSC's are consistent with the experimental observations for this series of HTSC's.

One of the drawbacks of the present study is that dT_c/dx for the different rare earths do not give a linear decrease (look at Table 4.1-4.6 and Figure 4.11-4.16). This was due to the use of alumel-chromel thermocouples to determine the temperature. Effort is now going on to employ a calibrate carbon glass thermometer to determine them.

REFERENCES

1. Kittel C. Introduction to solid state. 7th ed. Singapore: John Wiley and Sons; 1996.

2. Cyrot M, Pavuna D. Introduction to superconductivity and high-T_c materials. Singapore: World Scientific; 1992.

3. Rose-Innes AC, Rhoderick EH. Introduction to superconductivity. London: Pergamon Press; 1969.

4. Parks RD, editor. Superconductivity. vol 1. New York: Marcel Dekker; 1969.

5. Cooper LN. Phys Rev 1956; 104: 1189.

6. Bardeen J, Cooper LN, Schrieffer JR. Microscopic Theory of Superconducticity. Phys Rev 1957; 108: 1175-7.

7. Portis AM. Electrodynamic of high-temperature superconductors. Singapore: World Scientific; 1993. p 1-32.

8. Anderson PW. Phys Rev B 1959; 115: 2.

9. Gor'kov LP. Soviet Phys JETP 1958; 7: 505.

10. Bednorz JG, Muller KA. Possible High T_c Superconductivity in the Ba-La-Cu-O System. Z Phys B 1986; 64: 189.

11. Chu CW, Hor PH, Meng RL, Gao L, Huang ZJ, Wang YQ. Evidence for Superconductivity above 40 K in the La-Ba-Cu-O Compound System. Phys Rev Lett 1987; 58: 405-7.

12. Hikami S, Hirai T, Kagoshima S, Jpn J Appl Phys 1987; 26: L314.

13. Zhao ZX, Chen LQ, Chi CG, Huang YZ, Liu JX, Chen GH, et al. Kexue Tongbao 1987; 3: 177.

14 Wu MK, Ashbunn JR, Torng CJ, Hor PH, Meng RL, Gao L, et al. Superconductivity at 93 K in a New Mixed-Phase Y-Ba-Cu-O Compound System at Ambient Pressure. Phys Rev Lett 1987; 58: 908-10.

15. Hor PH, Gao L, Meng RL, Huang ZJ, Wang YQ, Forsta K, et al. High-Pressure Study of the New Y-Ba-Cu-O Superconducting Compound System. Phys Rev Lett 1987; 58: 911-2.

16. Maeda H, Tanaka Y, Fukutomi M, Asano T. Jpn J Appl Phys 1988; 27: L209.

17. Sheng ZZ, Hermann AM. Nature 1988; 332: 55.

18. Sheng ZZ, Hermann AM. Nature 1988; 332: 138.

19. Parkin SS, Lee VY, Nazzal AI, Savoy R, Beyers R, Placa SL. $Tl_1Ca_{n-1}Ba_2Cu_nO_{2n+3}$ (n = 1, 2, 3) : A New Class of Crystal Structures Exhibiting Volume Superconductivity at up to ≅ 110 K. Phys Rev Lett 1988; 61: 750-3.

20. Chu CW, Gao L, Chen F, Huang ZJ, Meng RL, Xue YY. Superconductivity above 150 K in $HgBa_2Ca_2Cu_3O_{8+\delta}$ at High Pressures. Nature 1993; 365: 323-4.

21. Ihara H, Hirabayashi M, Tanino H, Tokiwa K, Ozawa H, Akahama Y, et al. Jpn J Appl Phys 1993; 32: L1372.

22. Cava RJ, Batlogg B, Chen CH, Rietman EA, Zahurak SM, Werder DJ. Oxygen Stoichiometry, Superconductivity and Normal-State Properties of $YBa_2Cu_3O_{7-\delta}$. Nature 1987; 329: 423-5.

23. Xiao G, Streitz FH, Gavrin A, Du YW, Chein CL. Effect of Transition-Metal Elements on the Superconductivity of Y-Ba-Cu-O. Phys Rev B 1987; 35: 8782-4.

24. Zhai Y. J Phys Cond Mat 1993; 5: 3623.

25. Dharwadkar SF, Jakkal VS, Yakhmi JV, Gopalakrishnan LK, Lyer RM. X-Ray Diffraction Coupled Thermogravimetric Investigations of $YBa_2Cu_3O_{7-x}$. Solid State Commun 1987; 64: 1429-33.

26. Gabelica Z, Derouance EG, Vigneron JP, Lambin PH, Renier M, Lucas AA, et al. Oxygen Stoichiometry of $YBa_2Cu_3O_{6.5+x}$ Superconducting Phase Formed and Stabilized under Various Atmospheres : A TG-DTA-DTG Study. Sol State Commun 1987; 64: 1221-4.

27. Holland GF, Stacy AM. Acc Chem Res 1988; 21:8.

28. Tarascon JM, McKinnon WR, Greene LH, Hull GW, Vogel EM. Oxygen and Rare-Earth Doping of the 90-K Superconducting Perovskite $YBa_2Cu_3O_{7-x}$. Phys Rev B 1987; 36: 226-34.

29. Williams GVM, Tallon JL. Ion Size Effects on T_c and Interplanar Coupling in $RBa_2Cu_3O_{7-\delta}$. Physica C 1996; 258: 41-6.

30. Lin JG, Huang CY, Xue YY, Chu CW, Gao XW, Ho JC. Origin of the R-Ion Effect on T_c in $RBa_2Cu_3O_7$. Phys Rev B 1995; 51:12900-3.

31. Shafer MW, Penney T, Olson BL, Greene RL, Koch RH. Phys Rev B 1989; 39: 2914.

32. Yang KN, Dalschouch Y, Ferreira JM, Lu BW, Neumeir J, Torikachvili MS. High Temperature Superconductivity in Rare Earth (R) –Barium Copper Oxides $(RBa_2)Cu_3O_{9-\delta}$. Sol State Commun 1987; 63: 515-9.

33. Tang IM, Leelaprute S, Osotchan T. Correlation between the Orthorhombicity and the Transition Temperatures of the "123" Rare Earth Series Superconductors. Sol State Commun 1997; 103: 577-9.

34. Tarascon JM, Barboux P, Miceli PF, Greene LH, Hull GW. Structural and Physical Properties of the Metal (M) Substituted $YBa_2Cu_{3-x}M_xO_{7-y}$ Perovskite. Phys Rev B 1988; 37:7458-69.

35. Maeno Y, Tomita T, Kyogoku M, Awaji S, Oki YA, Hoshino K. Substitution for Copper in a High-T_c Superconductor $YBa_2Cu_3O_{7-\delta}$. Nature 1987; 328: 512-4.

36. Ata-Allah SS, Xu Y, Heiden CH. Effect of Zn Doping on the Superconductivity of $RBa_2Cu_{3-x}Zn_xO_{7-y}$ (R = Yb, Er, Y, Dy, Gd, Eu, Sm and Nd) Physica C 1994; 221:39-45.

37. Peng NH, Liang Wy. On the Distinct T_c Decrease Behaviours in Fe, Ni and Zn Doped $YBa_2Cu_3O_{7-\delta}$. Physica C 1994; 233:61-6.

38. Summana PP, Varadraju UV. Effect of 3d Substitution in the $RBa_2Cu_{3-x}M_xO_7$ (R = Sm, Dy; M = Fe, Ni and Zn) Systems : Implications of R Ion Dependence and Disorder. Phys Rev B 1996; 53:14637-46.

39. Harris DC, Hills ME, Hewston TA. Preparation, Iodometric Analysis, and Classroom Demonstration of Superconductivity in $YBa_2Cu_3O_{8-x}$. J Chem Educ 1987; 64: 847-50.

40. Tang IM, Osotchan T, Leelaprute S. Rare Earth Ion Size Dependence of the T_c of the "RE-123" HTSC within the (d+s)-Wave Description of their Superconducting State Phys Lett A 1998; 244: 442-8.

41. Tang IM, Charoenthai N, Thongruang R. Coupling of the Orthorhombic Distortion to the Depression of the T_c's due to Zn^{2+} Doping in the "RE-123" HTSC's : A (d+s) Wave Picture. Int J Mod Phys B 1999; 13: 2291-98.

APPENDICES

Appendix A : Green Functions for Superconductor

Superconductivity is complicated by the fact that the exist anomalous Green functions (G.F.). This arises from the fact that the Hamiltonian contains off-diagonal elements if the basis vectors of the Hilbert space are the eigen states of the normal metal.

Let G_0 to stand for the 2x2 Green functions for the superconductor in the absence of impurities (both normal and magnetic (to first order) impurities) and G to stand for the 2x2 Green functions in the presence of the impurities.

$$G_0 = \frac{1}{-\omega^2 - \varepsilon_F^2 - |\Delta|^2}\begin{pmatrix} i\omega + \varepsilon & -\Delta \\ -\Delta^* & i\omega - \varepsilon \end{pmatrix}$$

$$G = \frac{1}{-\tilde{\omega}^2 - \varepsilon_F^2 - |\Omega|^2}\begin{pmatrix} i\tilde{\omega} + \varepsilon & -\Omega \\ -\Omega^* & i\tilde{\omega} - \varepsilon \end{pmatrix}$$

$$G^{-1} = G_0^{-1} - \Sigma$$

where Σ is sum of all irreducible diagrammatic corrections (2x2 matrix).

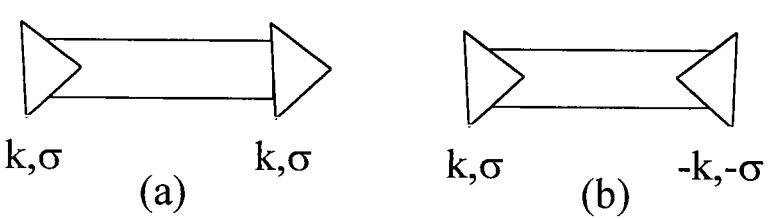

Figure A.1 Diagram for (a) diagonal propagator (b) off-diagonal propagator

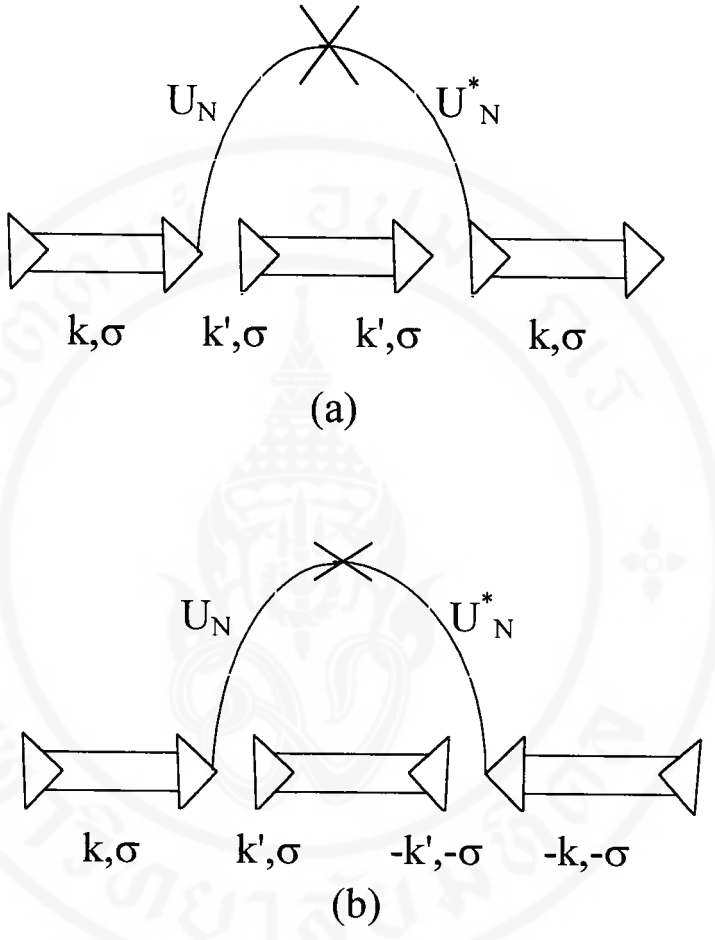

Figure A.2 Diagram for non-spin flip scattering (a) diagonal (b) off-diagonal

Analytic expression for non-spin flip scattering of diagonal term is

$$\tilde{\omega} = \omega + \frac{1}{2\tau_N} \frac{\omega}{\sqrt{\omega^2 + |\Phi|^2}}$$

And analytic expression for non-spin flip scattering of off-diagonal term is

$$\Omega = \Delta + \frac{1}{2\tau_N} \frac{\Phi}{\sqrt{\omega^2 + |\Phi|^2}}$$

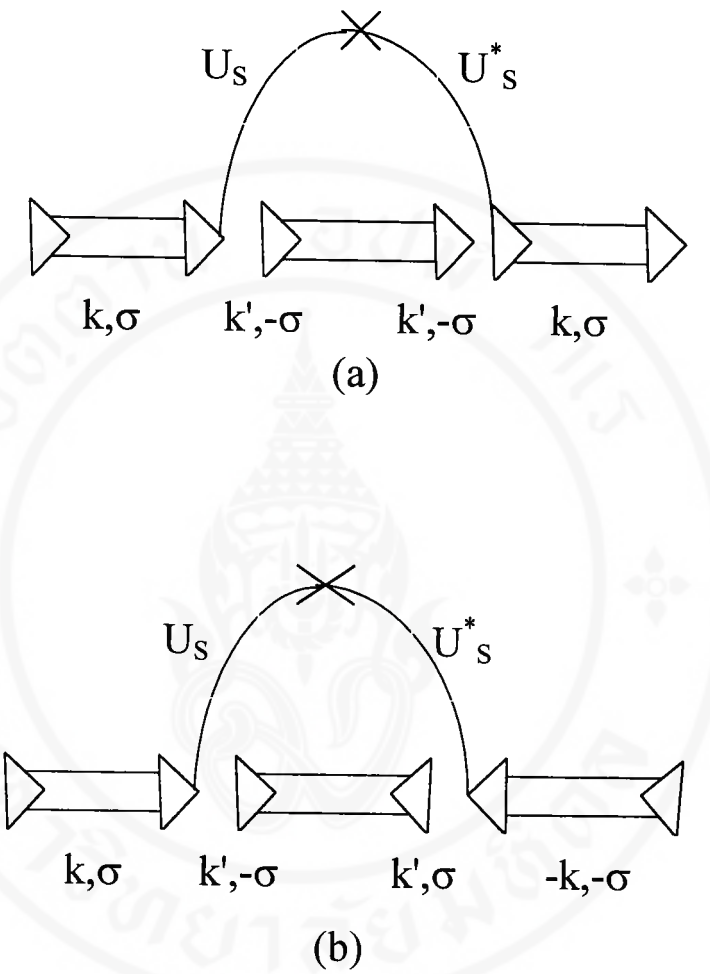

Figure A.3 Diagram for spin flip scattering (a) diagonal (b) off-diagonal

Analytic expression for spin flip scattering of diagonal term is

$$\tilde{\omega} = \omega + \frac{1}{2\tau_s} \frac{\omega}{\sqrt{\omega^2 + |\Phi|^2}}$$

And analytic expression for spin flip scattering of off-diagonal term is

$$\Omega = \Delta - \frac{1}{2\tau_s} \frac{\Phi}{\sqrt{\omega^2 + |\Phi|^2}}$$

where $\tilde{\omega}$ is unrenormalized frequency, ω is renormalized frequency, Ω is unrenormalized energy, Δ is renormalized energy , U_N is non spin flip scattering potential, U_S is spin flip scattering potential, τ_N is non spin flip scattering life time, and τ_S is spin flip scattering life time.

APPENDIX B

The Lattice parameters of $GdBa_2Cu_{3-x}Zn_xO_{7-y}$ calculated by IBMCENE as an example of the $REBa_2Cu_{3-x}Zn_xO_{7-y}$

$GdBa_2Cu_3O_{7-y}$

NAME OF SAMPLE GdBa2Cu3O7-y

INPUT THETA

SYSTEM ORTHORHOMBIC SYMMETRY

WEIGHTS WI WL^4/SIN2(2TH)

NO. OF ITERATION 4

CELL DIM. TO BE REFINED : A B C
A 3.83500
B 3.89470
C 11.67940

H	K	L	OBS	CAL	100000* OBS-CAL	WEIGHT WL = 1.54178
0	0	3	0.039068	0.039116	-4.78	37.63
0	1	0	0.039170	0.039240	-6.98	37.53
1	0	0	0.040467	0.040378	8.90	36.38
1	0	2	0.057791	0.057763	2.82	25.94
0	1	3	0.079953	0.078356	159.73	19.20
1	0	3	0.079480	0.079494	-1.34	19.31
0	0	5	0.108424	0.108656	-23.17	14.61
0	1	4	0.108696	0.108780	-8.37	14.58
1	1	3	0.118666	0.118734	-6.78	13.51
0	0	6	0.156139	0.156465	-32.55	10.72
0	2	0	0.156773	0.156959	-18.54	10.69
2	0	0	0.161562	0.161511	5.11	10.43
0	1	6	0.195273	0.195704	-43.13	8.99
1	1	6	0.235781	0.236082	-30.15	7.84
1	2	3	0.236151	0.236453	-30.13	7.83
0	1	7	0.253029	0.252206	82.33	7.47
0	2	6	0.313101	0.313423	-32.23	6.57
2	0	6	0.317968	0.317976	-0.78	6.51

CELL VOL 174.57686 NRREFL 18

	PARAMETER	STAND.DEV	PARAM. ----- ST.DEV	LASTSHIFT
A	3.83638	0.0051110	750	+3.13E-08
B	3.89161	0.0048217	807	-1.70E-08
C	11.69325	0.0101058	1157	+9.31E-08

$GdBa_2Cu_{2.998}Zn_{0.002}O_{7-y}$

NAME OF SAMPLE GdBa2Cu2.998Zn0.002O7-y

INPUT THETA

SYSTEM ORTHORHOMBIC SYMMETRY

WEIGHTS WI WL^4/SIN2(2TH)

NO. OF ITERATION 4

CELL DIM. TO BE REFINED : A B C
A 3.83500
B 3.89470
C 11.67940

H	K	L	OBS	CAL	100000* OBS-CAL	WEIGHT WL = 1.54178
0	0	3	0.039068	0.039109	-4.10	37.63
0	1	0	0.039170	0.039238	-6.81	37.53
1	0	0	0.040467	0.040378	8.83	36.38
1	0	2	0.057791	0.057760	3.06	25.94
0	1	3	0.079953	0.078347	160.58	19.20
1	0	3	0.079433	0.079488	-5.45	19.32
0	0	5	0.108370	0.108637	-26.70	14.62
0	1	4	0.108696	0.108766	-6.99	14.58
1	1	3	0.118609	0.118726	-11.64	13.51
0	0	6	0.156139	0.156437	-29.82	10.72
0	2	0	0.156773	0.156952	-17.87	10.69
2	0	0	0.161626	0.161514	11.27	10.43
0	1	6	0.195273	0.195675	-40.23	8.99
1	1	6	0.235781	0.236054	-27.31	7.84
1	2	3	0.236151	0.236440	-28.85	7.83
0	1	7	0.253029	0.252167	86.22	7.47
0	2	6	0.313020	0.313389	-36.92	6.57
2	0	6	0 317887	0.317951	-6.44	6.51

CELL VOL 174.59438 NRREFL 18

	PARAMETER	STAND.DEV	PARAM. ----- ST.DEV	LASTSHIFT
A	3.83635	0.0051577	743	+8.42E-08
B	3.89170	0.0048658	799	+1.49E-07
C	11.69428	0.0102002	1146	-1.39E-07

$GdBa_2Cu_{2.996}Zn_{0.004}O_{7-y}$

NAME OF SAMPLE GdBa2Cu2.996Zn0.0047-y

INPUT THETA

SYSTEM ORTHORHOMBIC SYMMETRY

WEIGHTS WI WL^4/SIN2(2TH)

NO. OF ITERATION 4

CELL DIM. TO BE REFINED : A B C
A 3.83500
B 3.89470
C 11.67940

H	K	L	OBS	CAL	100000* OBS-CAL	WEIGHT WL = 1.54178
0	0	3	0.039001	0.039110	-10.90	37.69
0	1	0	0.039170	0.039221	-5.14	37.53
1	0	0	0.040432	0.040357	7.49	36.41
1	0	2	0.057750	0.057739	1.07	25.96
0	1	3	0.079953	0.078331	162.21	19.20
1	0	3	0.079433	0.079467	-3.39	19.32
0	0	5	0.108316	0.108638	-32.24	14.63
0	1	4	0.108696	0.108750	-5.40	14.58
1	1	3	0.118609	0.118688	-7.91	13.51
0	0	6	0.156139	0.156439	-29.99	10.72
0	2	0	0.156710	0.156885	-17.54	10.69
2	0	0	0.161498	0.161429	6.82	10.43
0	1	6	0.195273	0.195660	-38.73	8.99
1	1	6	0.235781	0.236018	-23.71	7.84
1	2	3	0.236003	0.236352	-34.95	7.83
0	1	7	0.253029	0.252152	87.66	7.47
0	2	6	0.312939	0.313324	-38.51	6.57
2	0	6	0.317887	0.317869	1.79	6.51

CELL VOL 174.67601 NRREFL 18

	PARAMETER	STAND.DEV	PARAM. ----- ST.DEV	LASTSHIFT
A	3.83735	0.0052326	733	-8.68E-08
B	3.89252	0.0049361	788	-1.04E-07
C	11.69421	0.0103414	1130	+4.35E-07

$GdBa_2Cu_{2.994}Zn_{0.006}O_{7-y}$

NAME OF SAMPLE GdBa2Cu2.994Zn0.0067-y

INPUT THETA

SYSTEM ORTHORHOMBIC SYMMETRY

WEIGHTS WI WL^4/SIN2(2TH)

NO. OF ITERATION 4

CELL DIM. TO BE REFINED : A B C
A 3.83500
B 3.89470
C 11.67940

H	K	L	OBS	CAL	100000* OBS-CAL	WEIGHT WL = 1.54178
0	0	3	0.039068	0.039108	-3.95	37.63
0	1	0	0.039170	0.039231	-6.08	37.53
1	0	0	0.040467	0.040373	9.37	36.38
1	0	2	0.057791	0.057754	3.66	25.94
0	1	3	0.079953	0.078339	161.45	19.20
1	0	3	0.079433	0.079481	-4.77	19.32
0	0	5	0.108370	0.108633	-26.31	14.62
0	1	4	0.108696	0.108756	-6.01	14.58
1	1	3	0.118609	0.118712	-10.23	13.51
0	0	6	0.156139	0.156432	-29.25	10.72
0	2	0	0.156773	0.156923	-14.94	10.69
2	0	0	0.161626	0.161492	13.41	10.43
0	1	6	0.195273	0.195662	-38.93	8.99
1	1	6	0.235781	0.236035	-25.48	7.84
1	2	3	0.236077	0.236404	-32.65	7.83
0	1	7	0.253029	0.252152	87.72	7.47
0	2	6	0.312939	0.313354	-41.52	6.57
2	0	6	0.317805	0.317924	-11.86	6.52

CELL VOL 174.62544 NRREFL 18

	PARAMETER	STAND.DEV	PARAM. ----- ST.DEV	LASTSHIFT
A	3.83660	0.0051947	738	+2.84E-08
B	3.89206	0.0049010	794	-2.26E-08
C	11.69449	0.0102721	1138	+1.26E-07

$GdBa_2Cu_{2.992}Zn_{0.008}O_{7-y}$

NAME OF SAMPLE GdBa2Cu2.992Zn0.0087-y

INPUT THETA

SYSTEM ORTHORHOMBIC SYMMETRY

WEIGHTS WI WL^4/SIN2(2TH)

NO. OF ITERATION 4

CELL DIM. TO BE REFINED : A B C
A 3.83500
B 3.89470
C 11.67940

H	K	L	OBS	CAL	100000* OBS-CAL	WEIGHT WL = 1.54178
0	0	3	0.039001	0.039113	-11.18	37.69
0	1	0	0.039170	0.039209	-3.92	37.53
1	0	0	0.040432	0.040332	10.01	36.41
1	0	2	0.057750	0.057716	3.46	25.96
0	1	3	0.079906	0.078322	158.41	19.21
1	0	3	0.079386	0.079445	-5.87	19.33
0	0	5	0.108316	0.108646	-33.01	14.63
0	1	4	0.108696	0.108743	-4.67	14.58
1	1	3	0.118553	0.118654	-10.10	13.52
0	0	6	0.156139	0.156450	-31.10	10.72
0	2	0	0.156646	0.156837	-19.02	10.69
2	0	0	0.161369	0.161329	4.05	10.44
0	1	6	0.195273	0.195659	-38.63	8.99
1	1	6	0.235781	0.235992	-21.09	7.84
1	2	3	0.235929	0.236281	-35.25	7.84
0	1	7	0.253029	0.252155	87.37	7.47
0	2	6	0.312939	0.313287	-34.76	6.57
2	0	6	0.317805	0.317779	2.62	6.52

CELL VOL 174.75139 NRREFL 18

	PARAMETER	STAND.DEV	PARAM. ----- ST.DEV	LASTSHIFT
A	3.83854	0.0051463	745	-1.55E-08
B	3.89313	0.0048528	802	-5.10E-08
C	11.69380	0.0101619	1150	+3.23E-07

$GdBa_2Cu_{2.99}Zn_{0.010}O_{7-y}$

NAME OF SAMPLE GdBa2Cu2.99Zn0.010O7-y

INPUT THETA

SYSTEM ORTHORHOMBIC SYMMETRY

WEIGHTS WI WL^4/SIN2(2TH)

NO. OF ITERATION 4

CELL DIM. TO BE REFINED : A B C
A 3.83500
B 3.89470
C 11.67940

H	K	L	OBS	CAL	100000* OBS-CAL	WEIGHT WL = 1.54178
0	0	3	0.039035	0.039113	-7.88	37.66
0	1	0	0.039170	0.039207	-3.69	37.53
1	0	0	0.040467	0.040350	11.68	36.38
1	0	2	0.057791	0.057734	5.72	25.94
0	1	3	0.079906	0.078320	158.56	19.21
1	0	3	0.079480	0.079463	1.71	19.31
0	0	5	0.108316	0.108648	-33.24	14.63
0	1	4	0.108696	0.108742	-4.59	14.58
1	1	3	0.118553	0.118670	-11.73	13.52
0	0	6	0.156139	0.156454	-31.43	10.72
0	2	0	0.156646	0.156827	-18.09	10.69
2	0	0	0.161434	0.161400	3.38	10.44
0	1	6	0.195273	0.195660	-38.72	8.99
1	1	6	0.235781	0.236010	-22.96	7.84
1	2	3	0.235929	0.236291	-36.18	7.84
0	1	7	0.253029	0.252158	87.14	7.47
0	2	6	0.312939	0.313281	-34.16	6.57
2	0	6	0.317805	0.317853	-4.81	6.52

CELL VOL 174.71629 NRREFL 18

	PARAMETER	STAND.DEV	PARAM. ----- ST.DEV	LASTSHIFT
A	3.83770	0.0051478	745	+7.12E-08
B	3.89324	0.0048572	801	+1.05E-07
C	11.69367	0.0101700	1149	-3.72E-07

$GdBa_2Cu_{2.988}Zn_{0.012}O_{7-y}$

NAME OF SAMPLE GdBa2Cu2.988Zn0.012O7-y

INPUT THETA

SYSTEM ORTHORHOMBIC SYMMETRY

WEIGHTS WI WL^4/SIN2(2TH)

NO. OF ITERATION 4

CELL DIM. TO BE REFINED : A B C
A 3.83500
B 3.89470
C 11.67940

H	K	L	OBS	CAL	100000* OBS-CAL	WEIGHT WL = 1.54178
0	0	3	0.039001	0.039113	-11.17	37.69
0	1	0	0.039170	0.039208	-3.80	37.53
1	0	0	0.040432	0.040344	8.81	36.41
1	0	2	0.057750	0.057728	2.27	25.96
0	1	3	0.079906	0.078320	158.54	19.21
1	0	3	0.079480	0.079457	2.38	19.31
0	0	5	0.108316	0.108646	-32.99	14.63
0	1	4	0.108696	0.108741	-4.54	14.58
1	1	3	0.118553	0.118665	-11.18	13.52
0	0	6	0.156139	0.156450	-31.08	10.72
0	2	0	0.156646	0.156832	-18.54	10.69
2	0	0	0.161434	0.161377	5.68	10.44
0	1	6	0.195273	0.195658	-38.48	8.99
1	1	6	0.235781	0.236002	-22.14	7.84
1	2	3	0.235929	0.236289	-35.96	7.84
0	1	7	0.253029	0.252154	87.52	7.47
0	2	6	0.312939	0.313282	-34.25	6 57
2	0	6	0.317805	0.317827	-2.15	6.52

CELL VOL 174.72826 NRREFL 18

	PARAMETER	STAND.DEV	PARAM. ----- ST.DEV	LASTSHIFT
A	3.83797	0.0051445	746	-2.30E-07
B	3.89319	0.0048531	802	-9.05E-08
C	11.69381	0.0101621	1150	-2.29E-07

BIOGRAPHY

NAME	Lt.Jg. Nipaphat Charoenthai
DATE OF BIRTH	27 November 1971
PLACE OF BIRTH	Nakhonsawan Thailand
INSTITUTION ATTENED	Chaingmai University, 1989-1992: Bachelor of Science (Industrial Chemistry) Mahidol University, 1998-2000: Master of Science (Physical Chemistry)
RESEARCH GRANT	Institue of Science & Technology for Research & Development, Mahidol University, Nakorn Pathom, Thailand
POSITION & OFFICE	1996-Present,Dept of Chemistry, Faculty of Science, Naresuan University, Phitsanulok, Thailand